Mon. Not. R. Astron. Soc. **000**, 1–**??** (2002) Printed 3 October 2014 (MN LATEX style file v2.2)

Amplification of OAM Radiation by Astrophysical Masers

M. D. Gray[1], G. Pisano[1], S. Maccalli[1] and P. Schemmel[1]
[1]*Jodrell Bank Centre for Astrophysics, School of Physics and Astronomy, University of Manchester, M13 9PL, UK*

arXiv:1410.0643v1 [astro-ph.GA] 2 Oct 2014

ABSTRACT
We extend the theory of astrophysical maser propagation through a medium with a Zeeman-split molecular response to the case of a non-uniform magnetic field, and allow a component of the electric field of the radiation in the direction of propagation: a characteristic of radiation with orbital angular momentum. A classical reduction of the governing equations leads to a set of nine differential equations for the evolution of intensity-like parameters for each Fourier component of the radiation. Four of these parameters correspond to the standard Stokes parameters, whilst the other five represent the z-component of the electric field, and its coupling to the conventional components in the $x-y$-plane. A restricted analytical solution of the governing equations demonstrates a non-trivial coupling of the Stokes parameters to those representing orbital angular momentum: the z-component of the electric field can grow from a background in which only Stokes-I is non-zero. A numerical solution of the governing equations reveals radiation patterns with a radial and angular structure for the case of an ideal quadrupole magnetic field perpendicular to the propagation direction. In this ideal case generation of radiation orbital angular momentum, like polarization, can approach 100 per cent.

Key words: masers – radiative transfer – radio lines: general – radiation mechanisms: general – techniques: high angular resolution – ISM: lines and bands.

1 INTRODUCTION

The angular momentum carried by electromagnetic radiation is not limited to the familiar spin angular momentum, associated with polarization. It is also possible for radiation to exhibit orbital angular momentum (OAM) (Humblet 1943; Allen et al. 1992). Like other forms of electromagnetic radiation, light carrying OAM is often considered quantized into photons, and the OAM may then be referred to as photon-OAM (POAM). It appears to be a matter of debate as to whether the orbital and spin angular momenta are independently quantized: work in favour (Allen et al. 1992; Barnett 2002) is challenged in Grinter (2008) and references therein, where conservation applies to the total angular momentum and its projection on the propagation axis. Assuming that it is possible to make at least an approximate separation of spin and OAM, rays of radiation carrying well-defined amounts of OAM are referred to as helical modes. As with most work based on the radio waveband, it is convenient to consider the radiation in the form of classical fields, so from now on we will consider mostly OAM rather than POAM. A convenient distinction may be made in the manner of detection: POAM then refers to radiation that undergoes quantum detection, releasing a fixed amount of energy, whilst OAM refers to radio-style detection at the electric field level, with measurement of amplitude and phase.

Radiation with POAM is well known in astrophysics, even if not by this name: any quantized transition of an atom or molecule that is not an electric dipole transition can lead to the appearance of radiation carrying OAM: for example an electric quadrupole transition in a molecule, with a change in rotational quantum number of $\Delta J = \pm 2$, emits a photon with two units of angular momentum, only one of which can be spin. Such a photon is just one example from a hierarchy of electric multipole photons, corresponding to transitions of increasing numbers of quanta (Berestetskii et al. 1982). An example of such a transition is the $v = 1-0, S(1)$ transition of H_2 at 2.122 μm . As an S-branch transition, $\Delta J = 2$, and photons emitted in this transition must carry POAM in addition to spin. This transition has been observed from regions of shocked molecular hydrogen at least as far back as the mid-1980s (Gatley et al. 1984).

In the radio region, the familiar 21-cm line of atomic hydrogen (Ewen & Purcell 1951) must also be a carrier of POAM because it is emitted by a magnetic dipole transition. Although only one quantum of angular momentum is carried in this case, POAM is required to allow the photons to have even parity. In spite of this property of 21-cm photons, we do not expect typical HI observations to display an OAM signal - that is a spatial structure in the complex amplitude of the electric field that may be mathematically represented in terms of helical modes. Emission from most radio sources is simply too spatially incoherent, or chaotic, for any OAM signal to be found.

The OAM properties of a helical mode propagating along the z-axis, may be represented in terms of polar coordinates, r, ϕ in the xy-plane. The electric field of such a mode may be written,

$$\boldsymbol{E}(r,\phi) = \boldsymbol{E}_0(r)\mathrm{e}^{im\phi},$$

where m is an integer, known as the helicity of the mode. More complicated fields may be resolved into a superposition of helical

modes with a theoretically infinite range of m. Consequences of the helicity of the wave-fronts of modes with $m \neq 0$ include a Poynting vector that is not instantaneously parallel to the axis of propagation of the radiation, and that the electric field of the radiation includes a component parallel to the propagation axis (see for example, Allen et al. 1992; Padgett et al. 2004). Radiation with OAM of this type would not be detected by current radio telescopes due to rapid attenuation in the detector system (for single dish instruments) and a geographical phase offset (in interferometers).

In vacuum, or in homogeneous, isotropic media, spin and orbital angular momenta of radiation are conserved separately (Marrucci et al. 2006). Optically anisotropic media allow the exchange of the spin angular momentum with matter, but exchange of OAM with matter requires a transparent medium that is isotropic, but inhomogeneous. Anisotropic, inhomogeneous media allow OAM and spin angular momenta to be exchanged with matter simultaneously (Marrucci et al. 2006). In such a medium, the helicity of the output wave-front can be controlled by the polarization of the input radiation.

Practical devices for generating helical modes in the laboratory include astigmatically compensated laser cavities (Tamm & Weiss 1990; Santamato 2004), lens-based mode converters (Beijersbergen et al. 1993), computer-generated holograms (Bazhenov et al. 1992), spiral phase plates, for example Santamato (2004), and q-plates (Marrucci et al. 2006). The first of these can be considered a source of radiation with OAM, whilst the others convert a conventional beam into one or more helical modes. The operation of computer generated holograms, which resemble a diffraction grating with a fork discontinuity on the optical axis, is discussed in detail in Santamato (2004). A q-plate usually consists of a disc of ordinary dielectric material given birefringent properties by the incision of a set of azimuthal grooves. For the radio or microwave region, a disc of plastic is commonly used, for example nylon, refractive index n, with a radial groove periodicity smaller than $\lambda/2$, where λ is the operating wavelength. The diameter of the disc is $\gg \lambda$. Other important parameters of the q-plate, such as the groove depth, disc thickness and q itself, the space to period ratio, are related to λ, and controlled by formulae in Flanders (1983). Parameters for a radio astronomy device of this type may be found in Maccalli et al. (2013).

In astronomy, the passage of radiation with OAM through a variety of instruments has been considered by Elias (2008). In addition to free-space propagation, Elias considers reception by an aberration-free telescope, a coronagraph, a Michelson interferometer and a rancorimeter - a form of correlator. The present authors are constructing a q-plate-based detector to search for astrophysical signals with OAM in the microwave region: its parameters have been introduced above, and details appear in Maccalli et al. (2013). Harwit (2003) considers various possibilities for astrophysical sources of OAM-bearing radiation - one of which is the natural maser. Harwit (2003) suggests that OAM is imparted by significant departures of the refractive index from 1 within the volume of the maser - a feature of propagation rarely considered in studies of ideal maser amplification. A delay of order one wavelength can plausibly be reached in a distance much smaller than a typical maser gain length (10^{12} cm compared with 10^{14} cm) at the longer maser wavelengths (for example the 1.7-GHz lines of the OH rotational ground state). Moreover, this delay requires only a modest ionization fraction of $\sim 10^{-6}$ from cosmic rays. Other possible astrophysical generators of OAM include turbulent fields with Kolmogorov and von Karman spectra that lead to pairs of branch points, of opposite helicity, in a propagating electromagnetic wave (Sanchez & Oesch 2011a,b). Branch points of this type are formed by destructive interference of an initially plane wave passing through a turbulent medium of variable refractive index, and correspond to OAM photons (Oesch et al. 2012). The branch points also correspond to locations of zero intensity in wave-front sensors employed in the adaptive optics systems used with optical telescopes (Fried 1998). This property has enabled a real adaptive optics system to be used as an OAM-sensitve detector in the optical regime, and a first astronomical detection in this waveband has been convincingly claimed by Sanchez et al. (2013): they attempted to detect an OAM signal via an adaptive optics system towards a sample of five relatively nearby stars (within a few hundred pc of the Sun). A better than 3σ detection of OAM was obtained towards the K-type giant HR1529 with a conversion rate of an assumed OAM-free stellar flux to OAM on its journey to the detector of 7 per cent.

1.1 Diagnostic Value of OAM Radiation

The inclusion of parameters representing OAM should provide an advance in the diagnostic potential of radiation as great as that introduced by considering full polarization instead of intensity. Perhaps the best that can be said in general terms is that OAM radiation is diagnostic of inhomogeneities in the medium through which the radiation passes, both within an astronomical source, and in the interstellar medium. The inhomogeneities may be in density, velocity, gravitational fields or, in the context of the present work, magnetic fields.

As an example, consider the dispersion measure typically used in pulsar measurements: it tells us the column density of free electrons along a given line of sight, but we cannot tell if their distribution is smooth or clumpy. Even with a one part per million ionization level that might result from cosmic ray ionization, density inhomogeneitites can lead to variations in the refractive index of the medium. These can, in turn, lead to a 1-wavelength delay over a distance of order 10^{10} m for radiation of 20 cm wavelength, generating OAM (Harwit 2003). The fraction of radiation converted to OAM, and the spectrum of helical modes, index m, can tell us how clumpy the electron distribution is - information complementary to the standard dispersion measure. Harwit (2003) also state that the mode spectrum as a function of frequency may be used to distinguish between inhomogeneities in density, where the typical value of m is proportional to $1/\nu$, and gravitational inhomogeneities, where $m \propto \nu$.

Velocity and density inhomogeneities are often related through compressible turbulence, and passge of radiation through a turbulent medium has already resulted in the first astrophysical detections of OAM towards nearby stars (Sanchez et al. 2013; Oesch & Sanchez 2014). However, the information that can be obtained about the turbulence from OAM radiation is impressively detailed, including the velocity distribution in the sky plane, and the spatial distribution of the optical vortex pairs, resulting from positions where the gradient of the refractive index is very large.

It may also prove possible to detect rapidly rotating objects via OAM radiation scattered from their surfaces (Lavery et al. 2013). This diagnostic invokes a rotational form of the Doppler effect, and can detect rotation perpendicular to the line of sight. A frequency shift of $\Delta\nu = l\Omega/(2\pi)$ appears for an object with angular velocity Ω and radiation with l units of OAM.

1.2 Focus of the Present Work

In order to represent a system more closely related to previous studies of astrophysical maser environments, the present work considers the amplification of radiation with OAM by a non-uniform magnetic field, coupled to Zeeman-split molecular energy states. We note that there is a long history of theoretical studies of the propagation of polarized maser radiation through a Zeeman-split molecular ensemble generated by a uniform magnetic field (see below). Separately, non-uniform magnetic fields have been suggested as a generator for radiation with OAM (see for example Akamatsu & Kozuma 2003), without specific application to masers. We note that the Zeeman effect, even in a uniform magnetic field, renders the medium anisotropic, whilst introduction of non-uniformity makes it also inhomogeneous: properties that allow both spin and orbital angular momentum to be exchanged with the medium.

1.3 Earlier Zeeman Maser Studies

One of the most striking observational phenomena associated with OH masers in Galactic star-forming regions is their very high level (often $\sim$100 per cent) of polarization, particularly circular and elliptical polarization. An association of these polarization properties with magnetic fields and the Zeeman effect was suggested in the earliest days of astrophysical maser research (Weinreb et al. 1965). A theoretical description of the amplification and saturation of polarized masers in a medium of Zeeman-split molecules from an unsplit $J = 1 - 0$ transition was supplied by Goldreich et al. (1973). This description considers several cases, depending on whether the maser is in the limit of negligible or extreme saturation, and whether the magnetic field is sufficiently strong to provide a good quantization axis. However, it does not provide numerical results that show the development of polarization through arbitrary levels of saturation.

Advances in more recent studies include generalization to transitions more complicated than $J = 1 - 0$ (Western & Watson 1984; Deguchi & Watson 1990) together with numerical calculations covering arbitrary levels of saturation. The small and large Zeeman splitting limits have been developed to arbitrary splittings (Elitzur 1996) and the appearance of circular polarization as the Zeeman splitting is increased away from zero (Elitzur 1998; Watson & Wyld 2001). Propagation of polarized radiation through a more realistic medium, permeated by magnetohydrodynamic turbulence, has been considered by Wiebe & Watson (2007). More accurate saturation, with an attempt to include residual non-Gaussian statistics and coherence has been attempted by Gray & Field (1995) and Dinh-v-Trung (2009b). However, as far the present authors are aware, there has been no previous attempt to model the interaction of a molecular Zeeman system with radiation that has an electric field component in the direction of propagation: a necessary, but not sufficient, condition for the presence of an OAM radiation pattern. All that is known at present is that a uniform magnetic field can generate polarization, under some circumstances from an unpolarized background.

The polarized maser theory papers introduced above are not particularly consistent in the conventions they adopt with respect to the handedness of polarization, the definitions of the Stokes parameters, and the interpretation of the σ^+ and σ^- labels for transitions (see Section 2.7.1). All of the above can lead to minus signs entering equations that make interpretation difficult when comparing one theory paper with the works of other authors. An attempt to resolve some of the conventions used has been made by Green et al. (2014). In the present work we attempt to adhere strictly to the IEEE definition regarding the handedness of polarization, the IAU definition of Stokes-V, and the definition of $\sigma^{\pm}$ used by Garcia-Barreto et al. (1988).

1.4 Styles of Amplification

An astrophysical maser may generate radiation with an OAM angular pattern by two distinct processes that we will label active and passive amplification. Only active amplification will be considered further in the sections that follow the introduction.

In passive amplification, a thin slab of material sliced perpendicular to the propagation direction generates changes in the set of Stokes parameters, at each frequency in the lineshape, by interaction with the maser molecules in the medium. Some part of these changes is then converted into OAM via interaction with the non-uniform magnetic field only: there is no direct interaction of OAM radiation with the molecules. Passive amplification, if it occurs, is likely to be dominated by the saturated parts of a maser, simply on the grounds that these have high intensity, and there is more radiation to convert than when the maser is unsaturated.

In active amplification, we look for an interaction between the OAM radiation itself and the maser molecules. At first we consider only whether there can be a non-trivial coupling of the molecular response to a component of the electric field in the propagation direction: a component that does not exist for ordinary polarized radiation. Active amplification can, in principle, generate OAM from an OAM-free background, just as masers can, under the right geometrical, Zeeman and saturation conditions, produce high degrees of polarization from an unpolarized background.

Active amplification clearly requires radiation with OAM to induce stimulated emission in electric dipole molecular transitions. The theory developed below (Section 2) is semi-classical, with a quantum-mechanical molecular response driven by classical fields. From the classical field point of view, there is no problem: if a non-trivial coupling between the molecules and the electric field of the radiation is found, then the OAM radiation can drive the molecules. However, quantum-mechanically, it is not obvious that OAM radiation can drive electric dipole transitions at all: we expect, for example, that an electric quadrupole photon (which has one unit of OAM) to be unable to interact with electric dipole transitions with, say, $\Delta J = \pm 1$. Experimentally, however, It does appear that radiation with OAM can be made to interact with ordinary electric dipole transitions in the presence of a suitable non-uniform magnetic field (Akamatsu & Kozuma 2003). The magnetic field imposes a geometrical phase that allows the OAM to interact with the electric dipole moment of an atomic transition: in the case of Akamatsu & Kozuma (2003), the 795 nm D1 line of ^{87}Rb with $\Delta F = \pm 1$. It seems reasonable generally for photons photons with 2 units of OAM ($l = 2$) to interact with transitions that exchange one unit of angular momentum, since the photon has a total of three units of angular momentum: 2 of OAM and one of spin, and these can align to yield 1 unit to be exchanged with the atomic or molecular transition. However, the interaction is vastly weaker than for an $l = 0$ electric dipole photon (Grinter 2008).

2 THEORY

The theory here generalizes earlier polarized maser theory to the case of a non-uniform magnetic field and a non-zero compo-

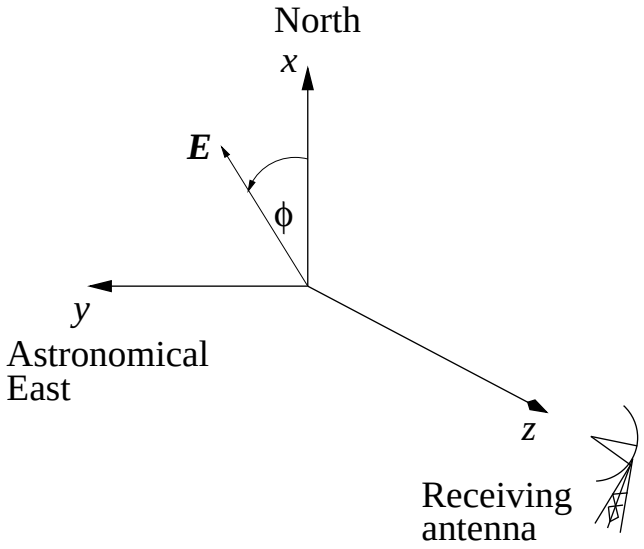

Figure 1. The global axis system, conforming to the IAU definition with the x-axis aligned to North and the y-axis to East. The electric field $\boldsymbol{E}$ is here shown in the xy-plane at angle ϕ from the x-axis.

nent of the electric field in the propagation direction: a necessary property of OAM modes. In particular, the theory follows Menegozzi & Lamb (1978), with additional polarization-specific detail from Dinh-v-Trung (2009b). Although the analysis is performed very generally, we consider results only in the limit of small signals, so that a classical reduction in terms of Stokes parameters is accurate, and a more advanced semi-classical saturation as used in Gray & Field (1995) is not required.

2.1 Axis Systems

We adopt a global, Cartesian, right-handed axis system, (x, y, z), based on the propagation direction of the radiation. Specifically, we use the standard IAU axis system (Hamaker & Bregman 1996) that is drawn in Fig. 1. Radiation propagates along the z-axis towards the observer, in a direction of increasing z. This definition is supplemented by a set of cylindrical polar coordinates, (r, ϕ, z), based on the same z-axis, with $r^2 = x^2 + y^2$ and $\phi = \arctan(y/x)$; the angle ϕ is measured anticlockwise from North.

The magnetic field, $\boldsymbol{B}$, is not uniform, so there can be no global system of coordinates based upon the magnetic field. Quantisation of angular momentum along an axis based on the magnetic field can therefore only be defined locally, that is at a specific point (r, ϕ, z). It will be assumed that the magnetic field is constant in time, but can be represented in the global coordinates as

$$\boldsymbol{B} = (B_x, B_y, B_z) = (B_r, B_\phi, B_z). \tag{1}$$

At any point (x, y, z) we define a local set of coordinates, also a right-handed Cartesian system, based on the local magnetic field. This is important from the point of view of defining the correct electric dipole alignments under the Zeeman effect (see Section 2.7.2). The local system is therefore,

$$(x', y', z') = (x'(x, y, z), y'(x, y, z), z'(x, y, z)),$$

and is arranged at each point such that

$$\boldsymbol{B} = B\boldsymbol{z}'(x, y, z). \tag{2}$$

Without loss of generality, we can specify one local axis to lie in the xy-plane, and we will choose the x'-axis for this purpose. Two rotations are therefore required to represent a vector defined in the (x, y, z) system to one in the local (x', y', z') system: a rotation through an angle ϕ' about the z-axis to an intermediate system (x^I, y^I, z^I) in which x^I is now aligned with x' and (y^I, z^I) is coplanar with (y', z'), followed by a rotation through θ about the x^I axis to align (y^I, z^I) with (y', z'). Both rotations are anticlockwise viewed in the direction of decreasing z (for the first rotation), or x' (for the second). The rotations are drawn in Fig. 2, noting that the vector (x, y, z) remains unchanged. The matrices corresponding to these rotations are defined in, for example, Arfken (1970) and known here as $\mathbf{R}_z(\phi')$ and $\mathbf{R}_{x'}(\theta)$. Applied sequentially, these matrices give us,

$$\begin{pmatrix} x' \\ y' \\ z' \end{pmatrix} = \mathbf{R}_{x'}(\theta)\mathbf{R}_z(\phi') \begin{pmatrix} x \\ y \\ z \end{pmatrix},$$

and we can combine these two matrices into the single product $\mathbf{R}(\theta, \phi') = \mathbf{R}_{x'}(\theta)\mathbf{R}_z(\phi')$, where

$$\mathbf{R} = \begin{pmatrix} 1 & 0 & 0 \\ 0 & \cos\theta & \sin\theta \\ 0 & -\sin\theta & \cos\theta \end{pmatrix} \begin{pmatrix} \cos\phi' & \sin\phi' & 0 \\ -\sin\phi' & \cos\phi' & 0 \\ 0 & 0 & 1 \end{pmatrix},$$

and evaluating this product, we obtain the overall rotation matrix,

$$\mathbf{R}(\theta, \phi') = \begin{pmatrix} \cos\phi' & \sin\phi' & 0 \\ -\cos\theta\sin\phi' & \cos\theta\cos\phi' & \sin\theta \\ \sin\theta\sin\phi' & -\sin\theta\cos\phi' & \cos\theta \end{pmatrix}, \tag{3}$$

with inverse,

$$\mathbf{R}^{-1}(\theta, \phi') = \begin{pmatrix} \cos\phi' & -\cos\theta\sin\phi' & \sin\theta\sin\phi' \\ \sin\phi' & \cos\theta\cos\phi' & -\sin\theta\cos\phi' \\ 0 & \sin\theta & \cos\theta \end{pmatrix}, \tag{4}$$

noting that $\mathbf{R}^{-1}$ operates on a vector in the primed (magnetic field) axis system, yielding its components in the unprimed (radiation) system. If we choose, for example, the unit vector $\hat{\boldsymbol{z}}' = (0, 0, 1)$ and use this as the right hand side of the rotation,

$$(x, y, z)^{\mathrm{T}} = \mathbf{R}^{-1}(\theta, \phi')(0, 0, 1)^{\mathrm{T}},$$

we find that the unit vector from the primed system has the unprimed coordinates,

$$\hat{\boldsymbol{z}}' = \hat{\boldsymbol{z}}\sin\theta\sin\phi' - \hat{\boldsymbol{y}}\sin\theta\cos\phi' + \hat{\boldsymbol{z}}\cos\theta.$$

On developing similar equations for $\hat{\boldsymbol{y}}'$ and $\hat{\boldsymbol{z}}'$, we find that a vector of unit vectors in the primed system transforms as

$$\begin{pmatrix} \hat{\boldsymbol{x}}' \\ \hat{\boldsymbol{y}}' \\ \hat{\boldsymbol{z}}' \end{pmatrix} = \begin{pmatrix} \cos\phi' & \sin\phi' & 0 \\ -\cos\theta\sin\phi' & \cos\theta\cos\phi' & \sin\theta \\ \sin\theta\sin\phi' & -\sin\theta\cos\phi' & \cos\theta \end{pmatrix} \begin{pmatrix} \hat{\boldsymbol{x}} \\ \hat{\boldsymbol{y}} \\ \hat{\boldsymbol{z}} \end{pmatrix}, \tag{5}$$

noting that the rotation matrix in eq.(5) is $\mathbf{R}$, rather than its inverse.

The angles θ and ϕ' may be calculated as follows: the dot product $\boldsymbol{B} \cdot \hat{\boldsymbol{z}} = B\cos\theta = B_z$, so if $B_z(x, y, z)$ is known from the global functional form of $\boldsymbol{B}$, then the angle is

$$\theta = \arccos(B_z/\sqrt{B_x^2 + B_y^2 + B_z^2}) = \arccos(B_z/B). \tag{6}$$

A vector in the xy-plane corresponding to the direction of $\hat{\boldsymbol{x}}'$ is given by the cross product of $\boldsymbol{B}$ on $\hat{\boldsymbol{z}}$, or $\boldsymbol{B} \times \hat{\boldsymbol{z}} = \hat{\boldsymbol{x}}B_y - \hat{\boldsymbol{y}}B_x$,

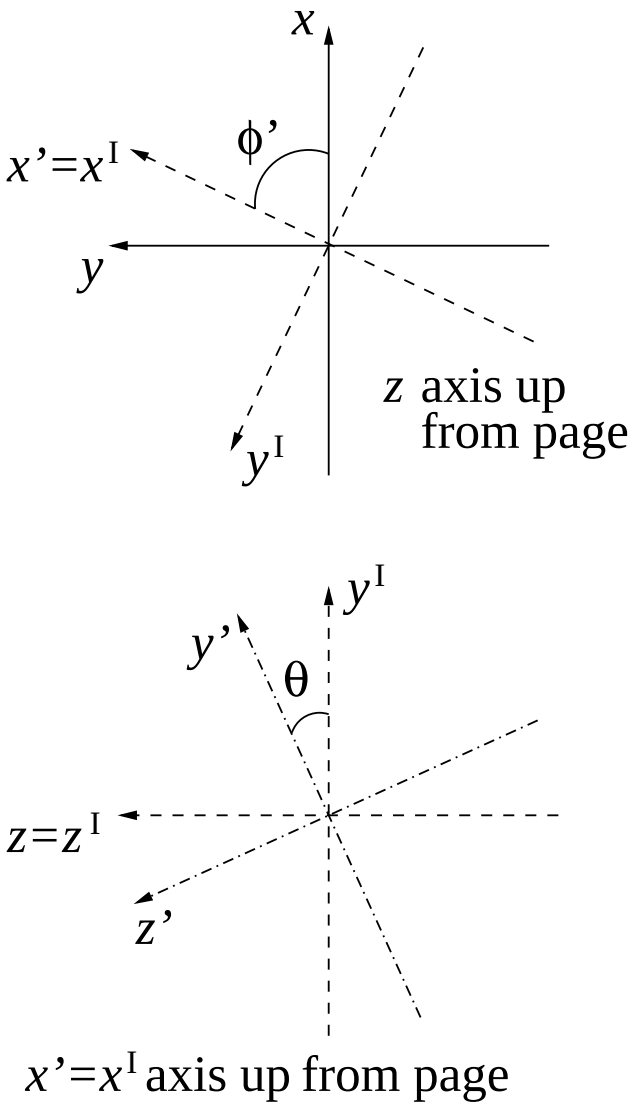

Figure 2. The two rotations required to specify the components of a vector (x, y, z) in the (x', y', z') system, leaving the vector itself unaffected. The rotation in the upper part of the figure is applied first.

and, because the magnitude of this result is $\sqrt{B_x^2 + B_y^2}$, the local $\hat{\boldsymbol{x}}'$ vector is,

$$\hat{\boldsymbol{x}}' = (\hat{\boldsymbol{x}} B_y - \hat{\boldsymbol{y}} B_x)/\sqrt{B_x^2 + B_y^2}. \tag{7}$$

The angle ϕ' is the offset between the $\hat{\boldsymbol{x}}$ and $\hat{\boldsymbol{x}}'$ unit vectors, and may therfore be calculated by dotting $\hat{\boldsymbol{x}}$ onto eq.(7) and setting the result equal to $\cos\phi'$. The angle is recovered as,

$$\phi' = \arccos(B_y/\sqrt{B_x^2 + B_y^2}). \tag{8}$$

2.1.1 Spherical Vector System

We have obtained a transformation of the Cartesian unit vectors as eq.(5). We now wish to re-write this transformation in terms of the spherical basis vectors that may be used to represent radiation polarization. We define these here, in terms of the Cartesian unit vectors, as

$$\hat{\boldsymbol{e}}_R = (\hat{\boldsymbol{x}} + i\hat{\boldsymbol{y}})/\sqrt{2} \tag{9a}$$

$$\hat{\boldsymbol{e}}_L = (\hat{\boldsymbol{x}} - i\hat{\boldsymbol{y}})/\sqrt{2}, \tag{9b}$$

a form that follows the definitions in Goldreich et al. (1973). The unit vector $\hat{\boldsymbol{z}}$ is common to both the spherical and Cartesian systems. In the local primed frame, exactly the same relationships apply, so that

$$\hat{\boldsymbol{e}}'_R = (\hat{\boldsymbol{x}}' + i\hat{\boldsymbol{y}}')/\sqrt{2} \tag{10a}$$

$$\hat{\boldsymbol{e}}'_L = (\hat{\boldsymbol{x}}' - i\hat{\boldsymbol{y}}')/\sqrt{2}. \tag{10b}$$

The definitions in eq.(9) may be inverted, yielding the Cartesian unit vectors,

$$\hat{\boldsymbol{x}} = (\hat{\boldsymbol{e}}_R + \hat{\boldsymbol{e}}_L)/\sqrt{2} \tag{11a}$$

$$\hat{\boldsymbol{y}} = -i(\hat{\boldsymbol{e}}_R - \hat{\boldsymbol{e}}_L)/\sqrt{2}, \tag{11b}$$

and similarly for the primed system. When we use eq.(11), and its primed counterpart, to eliminate $\hat{\boldsymbol{x}}$ and $\hat{\boldsymbol{y}}$ from eq.(5), we obtain the analogous expression in the spherical system This last equation is set as a two-column equation and may appear displaced from here.

2.2 The Electric field

We have noted in the Introduction that a distinguishing feature of radiation that carries OAM is a non-zero component of the electric field in the direction of propagation. We therefore write a general analytic signal for the radiation that includes all three Cartesian components:

$$\tilde{\boldsymbol{E}}(\boldsymbol{r}, t) = \hat{\boldsymbol{x}}\tilde{E}_x(\boldsymbol{r}, t) + \hat{\boldsymbol{y}}\tilde{E}_y(\boldsymbol{r}, t) + \hat{\boldsymbol{z}}\tilde{E}_z(\boldsymbol{r}, t), \tag{13}$$

where the tilde symbol over an electric field component indicates a complex-valued quantity. For this section, and that on radiative transfer, we use the general position vector $\boldsymbol{r}$, and only adopt problem-specific coordinates in Section 2.3.2. The real-valued electric field is simply the real part of the analytic signal,

$$\boldsymbol{E}(\boldsymbol{r}, t) = \Re\{\tilde{\boldsymbol{E}}(\boldsymbol{r}, t)\}. \tag{14}$$

The electric field that we consider has a total spectral width $\Delta\nu$ that is narrow in the sense that $\Delta\nu \ll \nu_0$, where ν_0 is some representative frequency within the band of width $\Delta\nu$. However, the radiation is broad-band in the sense that it is inhomgeneously broadened by the Doppler effect, such that $\Delta\nu$ vastly exceeds any frequency range directly determined by the molecular response (the homogeneous width). To deal with this, we extract from eq.(13) a rapidly oscillating term,

$$e^{-iY_0(\boldsymbol{r},t)} = e^{-i\omega_0(t - \hat{\boldsymbol{n}}\cdot\boldsymbol{r}/c)}, \tag{15}$$

where $\omega_0 = 2\pi\nu_0$, and $\hat{\boldsymbol{n}}$ is a unit vector in the direction of radiation propagation. To obtain the last form in eq.(15), we adopt the paraxial approximation of negligible beam divergence. In this case, even for radiation with OAM, the direction of propagation lies along a single axis, taken here to be the z axis. The instantaeous Poynting vector, however, is not aligned with $\hat{\boldsymbol{z}}$ (Allen & Padgett 2011). This extraction operation leaves eq.(13) in the form,

$$\tilde{\boldsymbol{E}}(\boldsymbol{r}, t) = [\hat{\boldsymbol{x}}\tilde{\mathcal{E}}_x(\boldsymbol{r}, t) + \hat{\boldsymbol{y}}\tilde{\mathcal{E}}_y(\boldsymbol{r}, t) + \hat{\boldsymbol{z}}\tilde{\mathcal{E}}_z(\boldsymbol{r}, t)]e^{-iY_0}, \tag{16}$$

where $\tilde{\mathcal{E}}_q(\boldsymbol{r}, t)$, for $q = x, y, z$, is a complex amplitude that now has only a slow variation in $\boldsymbol{r}$ and t in the sense that $\partial\tilde{\mathcal{E}}_q/\partial t \ll \omega_0\tilde{\mathcal{E}}_q$ and $|\boldsymbol{\nabla}\tilde{\mathcal{E}}_q| \ll \omega_0\tilde{\mathcal{E}}_q/c$.

Note that the choice of the sign e^{-iY_0} (rather than e^{+iY_0})

$$\begin{pmatrix} \hat{\boldsymbol{e}}'_R \\ \hat{\boldsymbol{z}}' \\ \hat{\boldsymbol{e}}'_L \end{pmatrix} = \begin{pmatrix} (1+\cos\theta)(\cos\phi' - i\sin\phi')/2 & (i\sin\theta)/\sqrt{2} & (1-\cos\theta)(\cos\phi' + i\sin\phi')/2 \\ \sin\theta(\sin\phi' + i\cos\phi')/\sqrt{2} & \cos\theta & \sin\theta(\sin\phi' - i\cos\phi') \\ (1-\cos\theta)(\cos\phi' - i\sin\phi')/2 & (-i\sin\theta)/\sqrt{2} & (1+\cos\theta)(\cos\phi' + i\sin\phi')/2 \end{pmatrix} \begin{pmatrix} \hat{\boldsymbol{e}}_R \\ \hat{\boldsymbol{z}} \\ \hat{\boldsymbol{e}}_L \end{pmatrix}. \quad (12)$$

in eq.(16) ensures that the spherical unit vectors from eq.(9) correctly represent right- and left-handed circular polarization under the IEEE convention (Hamaker & Bregman 1996). We will often use a representation of the electric field in terms of the spherical unit vectors, writing

$$\tilde{\boldsymbol{E}}(\boldsymbol{r},t) = [\hat{\boldsymbol{e}}_R\tilde{\mathcal{E}}_R(\boldsymbol{r},t) + \hat{\boldsymbol{e}}_L\tilde{\mathcal{E}}_L(\boldsymbol{r},t) + \hat{\boldsymbol{z}}\tilde{\mathcal{E}}_z(\boldsymbol{r},t)]e^{-iY_0}, \quad (17)$$

where the right- and left-handed complex amplitudes are found to be,

$$\tilde{\mathcal{E}}_R = (\tilde{\mathcal{E}}_x - i\tilde{\mathcal{E}}_y)/\sqrt{2} \quad (18a)$$

$$\tilde{\mathcal{E}}_L = (\tilde{\mathcal{E}}_x + i\tilde{\mathcal{E}}_y)/\sqrt{2}. \quad (18b)$$

2.2.1 Other OAM Representations

The representation of the electric field in eq.(16) is possibly unusual in studies of OAM radiation. It seems customary to adopt a representation, at least for laboratory studies, in terms of the Laguerre-Gaussian modes (L-G modes). These modes themselves are used to describe the electric and magnetic fields of the radiation perpendicular to the z axis, whilst the z-component of the field is proportional to x and y gradients of the L-G modes.

Our electric field must satisfy the wave-equation,

$$\nabla^2\boldsymbol{E} = \frac{\mu_r\epsilon_r(\boldsymbol{r})}{c^2}\frac{\partial^2\boldsymbol{E}}{\partial t^2}, \quad (19)$$

and we show below in Section 2.3 that the form in eq.(16) does. Various approximations have been made in obtaining eq.(19), notably a negligible conductivity in the medium, a linear (dielectric) response of the medium to the electric field of the radiation, constant charge density and constant value of μ_r, the relative permeability. However, μ_r could be a tensor constant, and ϵ_r could be a tensor quantity that is dependent on position (but not time). Equation 19 is separable into time and space parts by the multiplicative substitution,

$$\tilde{\boldsymbol{E}}(\boldsymbol{r},t) = \tilde{\boldsymbol{E}}_{\boldsymbol{r}}(\boldsymbol{r})\tilde{\boldsymbol{E}}_t(t). \quad (20)$$

The time part becomes a wave equation, whilst the spatial part reduces to a form of the Helmholtz equation. If the constant of separation is $-k^2$, where $\omega = kc$, then we can write one solution of the time part, corresponding to our choice of fast term in the analytic signal as,

$$\tilde{\boldsymbol{E}}_t(t) = Ae^{-i\omega t} = Ae^{-i\varpi t}e^{-i\omega_0 t}, \quad (21)$$

where $\varpi = \omega - \omega_0 << \omega$ is a small frequency within the spectral width $\Delta\nu$. We can further combine the constant amplitude A with the slowly-varying term as a complex amplitude,

$$\tilde{A}(t) = Ae^{-i\varpi t}. \quad (22)$$

The important point about this separation of variables is that we can write the electric field from eq.(20) as

$$\tilde{\boldsymbol{E}}(\boldsymbol{r},t) = [\hat{\boldsymbol{e}}_R\tilde{\mathcal{E}}_R(\boldsymbol{r}) + \hat{\boldsymbol{e}}_L\tilde{\mathcal{E}}_L(\boldsymbol{r}) + \hat{\boldsymbol{z}}\tilde{\mathcal{E}}_z(\boldsymbol{r})]e^{i\omega_0 z/c}\tilde{A}(t)e^{-i\omega_0 t}, \quad (23)$$

where the spatial part must satisfy a Helmholtz equation. If the relative permeability and permittivity are constant, the paraxial form of the Helmholtz equation may be solved via the LG modes, or any other suitable expansion for the spatial part of the electric field.. We adopt instead the electric field representation in eq.(16) because the relative permittivity in the current problem is not constant, and we solve the resulting radiative transfer problem in Section 2.3. The problem for which the LG modes are a solution may be considered a limit of this problem for free space or a homogeneous medium.

Another possibly useful field expansion is one in terms of the spherical harmonic vectors, $\boldsymbol{Y}^{(e)}_{J,M}$ and $\boldsymbol{Y}^{(m)}_{J,M}$, corresponding to electric (e) and magnetic (m) multipole photons of total angular momentum quantum number J and projection on the propagation axis M. The spherical harmonic vectors may be resolved into components along the propagation axis and perpendicular to it, the latter again resolved into components following $\hat{\boldsymbol{e}}_R$ and $\hat{\boldsymbol{e}}_L$ (Berestetskii et al. 1982). We note that the definitions of the spherical unit vectors differ by multiplicative constants from those used in the present work. OAM is present in all of the multipole photons except the electric dipole type.

2.2.2 Fourier Representation

The complex amplitudes in eq.(16) and eq.(17) are functions of position and time, but they can be considered as being constructed from all the frequencies within the spectral bandwidth. For a signal of infinite duration, we would integrate over a continuum of frequencies, corresponding to an idealized case of Fourier components of infinitessimal width. Astrophysical signals are limited in time by a sampling process at the telescope, so the Fourier components in a practical signal have a finite width of order $\delta\nu = 1/T$, where T is the sample duration.

The standard Fourier transform operations need some modification to work with a limited time range and Fourier components of finite width in the frequency domain. We adopt the transforms used by Menegozzi & Lamb (1978), and subsequently used by Dinh-v-Trung (2009b) and Gray (2012). The inverse transform, from frequency to time, becomes a sum over finite-width frequency strips, and a complex amplitude for Cartesian or spherical spatial component q is

$$\tilde{\mathcal{E}}_q(\boldsymbol{r},t) = (2\pi)^{-1}\sum_{n=-\infty}^{\infty}\tilde{\mathcal{E}}_q(\boldsymbol{r},\varpi_n)e^{-i\varpi_n(t-\hat{\boldsymbol{n}}\cdot\boldsymbol{r}/c)}, \quad (24)$$

where $\varpi_n = \omega_n - \omega_0$ is a local frequency of magnitude $\ll \omega_0$, corresponding to the centre of Fourier component n. Although the sum over the Fourier components has been formally written with infinite limits, the number of strips required to cover a certain number of inhomogeneous line widths, for example, would be a finite number. The forward transform, the inverse of that in eq.(24), transforming from the time domain to local frequency is

$$\tilde{\mathcal{E}}_q(\boldsymbol{r},\varpi_n) = T^{-1}\int_{-T/2}^{T/2}\tilde{\mathcal{E}}_q(\boldsymbol{r},t)e^{i\varpi_n(t-\hat{\boldsymbol{n}}\cdot\boldsymbol{r}/c)}. \quad (25)$$

These transformations will be used extensively in Section 4.

2.3 Radiative Transfer

The electric field introduced in Section 2.2 must satisfy the wave equation

$$\nabla^2 \boldsymbol{E} = \frac{\mu_0 \epsilon_r(\boldsymbol{r})}{c^2} \frac{\partial^2 \boldsymbol{E}}{\partial t^2}, \tag{26}$$

, that follows from eq.(19), but we have now assumed a relative permeability of 1. The relative permittivity ϵ_r may be a scalar or tensor quantity. We assume that the propagation medium is dielectric, so that the macroscopic polarization of the medium, $\boldsymbol{P}(\boldsymbol{r}, t)$, is linearly related to the electric field via the formula

$$\boldsymbol{P}(\boldsymbol{r}, t) = \epsilon_0(\epsilon_r(\boldsymbol{r}) - 1)\boldsymbol{E}(\boldsymbol{r}, t). \tag{27}$$

Equation 27 may be used to eliminate the permittivity from eq.(26), leaving a wave equation in terms of $\boldsymbol{P}$:

$$\nabla^2 \boldsymbol{E} = \frac{1}{c^2} \frac{\partial^2 \boldsymbol{E}}{\partial t^2} + \mu_0 \frac{\partial^2 \boldsymbol{P}}{\partial t^2}. \tag{28}$$

We now substitute the electric field, in the anlytic signal representation of eq.(13), into eq.(28), assuming that the same representation can be used for $\boldsymbol{P}$. It immediately breaks down into three scalar equations for the Cartesian components of the field. If each Cartesian component is then put into the form used in eq.(16), the various derivatives can be calculated and substituted into each scalar wave equation. After some algebra, the details of which may be found in Gray (2012), the rapidly oscillating terms are lost, and we find that the complex amplitude of Cartesian component q of the electric field is transferred according to,

$$\left(\frac{\partial}{\partial t} + c\hat{\boldsymbol{n}} \cdot \boldsymbol{\nabla} \right) \tilde{\mathcal{E}}_q = \frac{i\omega_0}{2\epsilon_0} \tilde{\mathcal{P}}_q, \tag{29}$$

where $\tilde{\mathcal{P}}_q$ is the complex amplitude of the macroscopic polarization that relates to $\tilde{P}_q$ as $\tilde{\mathcal{E}}_q$ relates to $\tilde{E}_q$. The form of eq.(29) is in accord with Goldreich et al. (1973), who also include a macroscopic magnetization.

2.3.1 Macroscopic Polarization

The macroscopic polarization is the velocity-integrated expectation value of the electric dipole operator of the active molecule that amplifies the maser. It is a reasonably general result from quantum-mechanics that such an expectation value is the trace of the matrix product of the molecular density matrix (DM) and the operator. Writing the dipole operator as $\hat{\mathbf{d}}$, the expectation value is therefore $\langle \hat{\mathbf{d}} \rangle = \mathrm{Tr}[\rho \hat{\mathbf{d}}]$, where $\rho(\boldsymbol{r}, t, \boldsymbol{v})$ is the molecular DM, a function of molecular velocity $\boldsymbol{v}$ as well as position and time. Note that the row and column indices of these matrices correspond to energy levels of the molecule and that, in the case of the dipole, its individual elements, $\hat{\boldsymbol{d}}_{pq}$ are themselves vectors. To obtain the macroscopic polarization we must integrate over the molecular velocity to obtain,

$$\boldsymbol{P}(\boldsymbol{r}, t) = \int_{\boldsymbol{v}} d^3v \mathrm{Tr}[\rho(\boldsymbol{r}, t, \boldsymbol{v}) \hat{\mathbf{d}}]. \tag{30}$$

By isolating one component of the macroscopic polarization, changing to an analytic signal representation, and using the standard representation of the trace of a matrix product in terms of individual elements, one Cartesian component of the complex amplitude of $\boldsymbol{P}$ may be written as

$$\tilde{\mathcal{P}}_q = 2e^{iY_0} \sum_{p=2}^{N} \sum_{k=1}^{p-1} \hat{d}^*_{pk,q} \int_{\boldsymbol{v}} \rho_{pk} d^3v. \tag{31}$$

where p and q represent molecular energy levels from a total of N, and $\hat{d}_{pk,q}$ is the Cartesian component q of the element pq of the density matrix. To remove the rapidly varying factor in eq.(31) we write the off-diagonal element of the DM as the product of a slowly varying part s_{pk} and a rapidly oscillating term as follows (Menegozzi & Lamb 1978):

$$\rho_{pk}(\boldsymbol{r}, t, v) = -(i/2) s_{pk}(\boldsymbol{r}, t, v) e^{-iY_0}. \tag{32}$$

Substitution of eq.(32) into eq.(31), and substiution of the result in turn into eq.(29) yields the radiative transfer equation,

$$\left(\frac{\partial}{\partial t} + c\hat{\boldsymbol{n}} \cdot \boldsymbol{\nabla} \right) \tilde{\mathcal{E}}_q(\boldsymbol{r}, t) = \frac{\omega_0}{2\epsilon_0} \sum_{p=2}^{N} \sum_{k=1}^{p-1} \hat{d}^*_{pk,q} \int_{\boldsymbol{v}} s_{pk}(\boldsymbol{r}, t, \boldsymbol{v}) d^3v. \tag{33}$$

2.3.2 Simplifications

So far, we have kept our description of the electric field and its transfer very general. At this point, however, we introduce some useful simplifications resulting from the geometry adopted in Section 2.1. The radiation is assumed to propagate along the z axis, in the direction of increasing z: therefore $\hat{\boldsymbol{n}} = \hat{\boldsymbol{z}}$. We can therefore reduce our transfer equation, eq.(33) to

$$d_t \tilde{\mathcal{E}}_q(r, \phi, z, t) = \frac{\omega_0}{2\epsilon_0} \sum_{p=2}^{N} \sum_{k=1}^{p-1} \hat{d}^*_{pk,q} \int_{-\infty}^{\infty} s_{pk}(r, \phi, z, t, v) dv. \tag{34}$$

The derivative on the left-hand side of eq.(34) is the shorthand notation,

$$d_t = \partial/\partial t + c\partial/\partial z, \tag{35}$$

the general position $\boldsymbol{r}$ has been replaced by the global (r, ϕ, z) cylindrical coordinates of Section 2.1, and we now consider only the z-component of the molecular velocity, $v = v_z$, since only the Doppler effect along the axis of propagation is observable. It is straightforward to show that eq.(34) applies to spherical, as well as Cartesian, components.

In the definition of the electric field, we re-define Y_0 as

$$Y_0 = \omega_0(t - z/c), \tag{36}$$

and with this modification, we may still use eq.(16) and eq.(17) to represent the analytic signal. We will also sometimes need a form in Cartesian components, but in terms of the spherical complex amplitudes, for example

$$\tilde{\boldsymbol{E}}(r, \phi, z, t) = 2^{-1/2}[\hat{\boldsymbol{x}}(\tilde{\mathcal{E}}_R + \tilde{\mathcal{E}}_L) + i\hat{\boldsymbol{y}}(\tilde{\mathcal{E}}_R - \tilde{\mathcal{E}}_L) + \sqrt{2}\hat{\boldsymbol{z}}\tilde{\mathcal{E}}_z] e^{-iY_0}. \tag{37}$$

2.4 Molecular Response

Equations for the evolution of general diagonal and off-diagonal elements of the molecular DM are taken from Gray (2012), where they are derived in detail from Schrödinger's equation. For the diagonal element, ρ_{qq},

$$D_t \rho_{qq} = \frac{i}{\hbar} \sum_{j=1}^{N} (\rho_{qj} \hat{H}_{jq} - \rho_{jq} \hat{H}_{qj}) + \sum_{j=1}^{N} (k_{jq} \rho_{jj} - k_{qj} \rho_{qq}), \tag{38}$$

noting that a diagonal element represents the number density of molecules in level q, or, in a normalised form, the probability of

occupancy of level q. The equation also makes use of off-diagonal elements of the DM, for example ρ_{pq}, where $p \neq q$, that represent coherence between pairs of levels from the total of N. Coupling to the maser radiation field is delivered through the matrix elements of the interaction Hamiltonian, $\hat{H}_{pq}$, and to other forms of level-changing process, such as kinetic collisions, via the all-process rate coefficients, k_{pq}. The total derivative is now,

$$D_t = \partial/\partial t + v\partial/\partial z, \tag{39}$$

noting that a molecular z-velocity, v, now replaces the speed of light used in radiative transfer equations (see eq.(35)). The diagonal elements of the DM have the functional dependence,

$$\rho_{qq} = \rho_{qq}(r, \phi, z, t, v). \tag{40}$$

The general off-diagonal element, ρ_{pq}, evolves according to the equation

$$D_t \rho_{pq} = \frac{i}{\hbar} \sum_{j=1}^{N} (\rho_{pj} \hat{H}^*_{qj} - \rho_{jq} \hat{H}_{pj}) - i\omega_{pq}\rho_{pq} - \rho_{pq}/\tau_{pq}. \tag{41}$$

A complex-conjugate version of an interaction Hamiltonian element has been used, noting that, like the DM, $\hat{\mathrm{H}}$ is Hermitian. In eq.(41) we also take p (q) to be the upper (lower) level of the pair, so that the angular frequency ω_{pq}, corresponding to the transition energy between the levels, is positive, and $\omega_{qp} = -\omega_{pq}$. The timescale τ_{pq} is the timescale over which coherence in the transition pq is lost. This will in general be shorter than $1/k_{pq}$ because it includes elastic processes, such as collisions that change molecular direction but not level. The functional dependence of the off-diagonal element is the same as for the diagonal element in eq.(40)

2.5 Off-Diagonal Equation: Modifications

We define the population inversion between upper level p and lower level q as

$$\Delta_{pq}(r, \phi, z, t, v) = \rho_{pp} - \rho_{qq}, \tag{42}$$

and isolate it from off-diagonal elements. To do this, we extract from the sum in eq.(41) those terms where $j = p$ and $j = q$, and write them separately. Since elements of the interaction Hamiltonian are defined by the equation,

$$\hat{H}_{pq}(r, \phi, z, t) = -\boldsymbol{E}(r, \phi, z, t) \cdot \hat{\boldsymbol{d}}_{pq}, \tag{43}$$

any element of the form $\hat{H}_{jj} = 0$ because the dipole $\hat{\boldsymbol{d}}_{jj} = 0$. Using this fact, and with the help of eq.(39), eq.(42) and the Hermitian property of $\hat{H}_{qp}$, we may write eq.(41) in the modified form,

$$D_t \rho_{pq} = \frac{i}{\hbar} \sum_{j \neq p,q}^{N} (\rho_{pj} \hat{H}^*_{qj} - \rho_{jq} \hat{H}_{pj}) + \frac{i\hat{H}_{pq}\Delta_{pq}}{\hbar} - (i\omega_{pq} + \gamma_{pq})\rho_{pq}, \tag{44}$$

where the homogeneous line width $\gamma_{pq} = 1/T_{pq}$.

2.6 Diagonal Equation: Modifications

To replace equations describing the evolution of individual level populations with equations that describe the evolution of an inversion, we write down a version of eq.(38) in which q is replaced by p, and subtract the original eq.(38) from it. Equation 42 dictates that the left-hand side of the result becomes the differential of the inversion Δ_{pq}. Using the Hermitian property of both the interaction Hamiltonian and DM, the result of the subtraction is

$$D_t \Delta_{pq} = \frac{-2}{\hbar} \sum_{j=1}^{N} (\Im\{\rho_{pj}\hat{H}_{jp}\} - \Im\{\rho_{qj}\hat{H}_{jq}\}) + \sum_{j=1}^{N} \rho_{jj}\Delta k_{j,pq} - \rho_{pp}k_{p\Sigma} + \rho_{qq}k_{q\Sigma}, \tag{45}$$

where we have defined $k_{p\Sigma} = \sum_{j=1}^{N} k_{pj}$ for the total rate-coefficient out of level p (and similarly for level q), and where $\Delta k_{j,pq} = k_{jp} - k_{jq}$. On the basis that the total rate coefficient out of any level is approximately the same, we make the approximation $k_{p\Sigma} \sim k_{q\Sigma} \sim \Gamma_{pq}$, where Γ_{pq} is the transition loss rate. The term in $\Delta k_{j,pq}$ represents a source term for the inversion, arising from all the remaining levels ρ_{jj}. We set it equal to a phenomenological pumping term,

$$\sum_{j=1}^{N} \rho_{jj}\Delta k_{j,pq} = P_{pq}\phi(\boldsymbol{v}), \tag{46}$$

where P_{pq} is the pumping constant for the pq inversion and $\phi(\boldsymbol{v})$ is the molecular velocity distribution function. The appearance of this distribution function in eq.(46) is justified on the grounds that the left-hand side contains the populations $\rho_{jj}(r, \phi, z, t, \boldsymbol{v})$ that all follow this distribution.

Extracting the $j = p$ and $j = q$ terms from the sum in eq.(45), and employing the Hermitian property of $\hat{\mathbf{H}}$, together with eq.(39), eq.(42) and eq.(46), the inversion evolves according to

$$D_t \Delta_{pq} = -\frac{2}{\hbar} \Im \left\{ 2\rho_{pq}\hat{H}_{qp} + \sum_{j \neq p,q}^{N} (\rho_{pj}\hat{H}_{jp} - \rho_{qj}\hat{H}_{jq}) \right\} + P_{pq}\phi(\boldsymbol{v}) - \Gamma_{pq}\Delta_{pq}. \tag{47}$$

From here on, we will assume that the molecular velocity distribution is a Gaussian function of the form,

$$\phi(\boldsymbol{v}) = (\pi^{1/2}w)^{-1} e^{-v^2/w^2}, \tag{48}$$

where w is a width parameter given by

$$w = (2k_B T_K/m_X)^{1/2}, \tag{49}$$

for kinetic temperature T_K and molecular mass of the maser molecule, m_X. Note that $\phi(\boldsymbol{v})$ can be changed only by molecular collisions and not by the Zeeman effect or by saturation or any other process within the maser.

2.7 Zeeman Patterns

We consider a weak-field Zeeman effect in which the the energy shift is proportional to the external field strength. Much more complicated patterns have been considered, for example by Asensio Ramos & Trujillo Bueno (2006), but not in connection with masers. We will also assume that the (local) magnetic field direction provides a good quantization axis. We will attempt to use a generic system where the maser molecule has a magnetic moment

$$\boldsymbol{m}_J = -\mu_X g_J \boldsymbol{J}, \tag{50}$$

where the magneton, μ_X, is the nuclear magneton, $e\hbar/(2m_p)$, for closed-shell molecules. For molecules like OH, with net electronic angular momentum, the Bohr magneton is used, replacing the proton mass m_p with the electron mass m_e in the formula above. The angular momentum $\boldsymbol{J}$ would be replaced by $\boldsymbol{F}$ in the case of OH (Dousmanis et al. 1955). We also assume that the Landé factor, g_J,

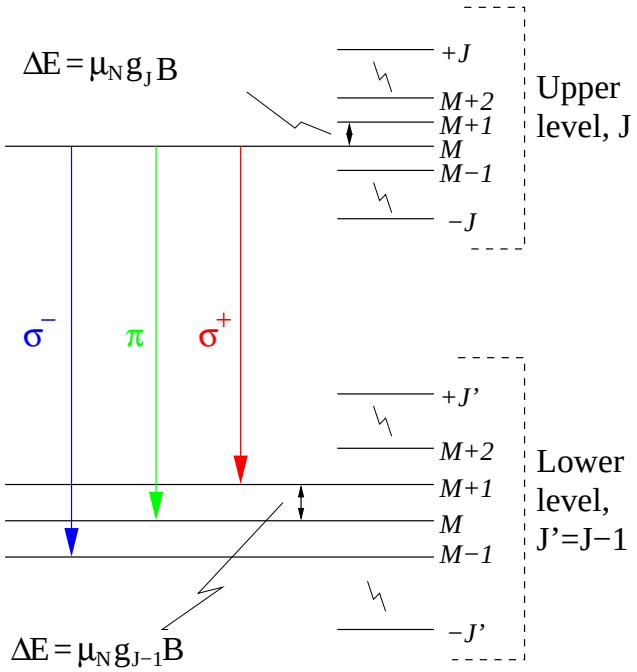

Figure 3. The Zeeman sub-levels of the two-level system considered in this work; the magnetic moment is anti-parallel to $\boldsymbol{J}$. The three possible electric-dipole transitions in emission from sublevel M of the upper rotational state are shown as coloured vertical arrows. Note that there is only one such transition of each type. Zeeman energy shifts are also shown.

is a positive number in eq.(50), so that the magnetic moment lies anti-parallel to $\boldsymbol{J}$. Our Zeeman pattern therefore follows, in sign, the usual 'textbook' case of electronic angular momentum. If $\boldsymbol{J}$ results mostly from molecular rotation, we are therefore assuming that the contribution to g_J from the coupling to the electron cloud has a greater magnitude than the contribution from the nuclear framework.

The Zeeman Hamiltonian for a molecule with magnetic moment $\boldsymbol{m}_J$ in an external magnetic field $\boldsymbol{B}$ is

$$H_Z = -\boldsymbol{m} \cdot \boldsymbol{B} \tag{51}$$

(Woodgate 1980; Eisberg & Resnick 1985; Gray 2012). The resulting Zeeman energy shift is

$$\Delta E(J, M) = \mu_X g_J B M, \tag{52}$$

where $B(x, y, z) = |\boldsymbol{B}|$ is the local magnetic field strength, and M is the magnetic quantum number that has integer values in the range $-J..0..+J$, where J is the quantum number corresponding to $\boldsymbol{J}$. An unsplit level denoted by J is therefore split by the external magnetic field into $2J + 1$ equally spaced Zeeman sublevels.

2.7.1 *Transition Types*

We will consider a pair of unsplit levels: an upper level J and lower level $J' = J - 1$, and take an idealised case where these are isolated from any other levels. Both of these unsplit levels then contain magnetic sublevels M, ranging from $-J$ to $+J$ in the upper level and from $-J'$ to $+J'$ in the lower level. Transitions between magnetic sub-levels of J and J' are subject to the electric dipole selection rules: $\Delta M = 0, \pm 1$ (Figure 3).

The allowed transitions will be classified as follows: let ΔM be the change in M in emission. A transition with $\Delta M = 0$ will be termed a π-transition. Transitions with $\Delta M = +1$ ($\Delta M = -1$) will be called σ^+ (σ^-) transitions. Note that any sublevel M in J can have at most one electric-dipole allowed transition of each type leaving it for some destination magnetic sub-level within J' (see Figure 3). Note that this classification of the σ transitions is not universal and that Goldreich et al. (1973), in particular, use the reverse definition.

The energy of our upper energy level with quantum numbers J, M, relative to a gound level of zero, is just the energy E_J of the unsplit rotational level added to the Zeeman shift from eq.(52):

$$E(J, M) = E_J + \mu_X g_J B M, \tag{53}$$

whilst the energies of the three target sub-levels in $J' = J - 1$ become

$$E(J-1, M) = E_{J-1} + \mu_X g_{J-1} B M \tag{54a}$$

$$E(J-1, M \pm 1) = E_{J-1} + \mu_X g_{J-1} B (M \pm 1). \tag{54b}$$

The frequency of the π-transition, ν^0_M, may be found by subtracting eq.(54a) from eq.(53) and dividing through by Planck's constant. If we let the frequency of the unsplit transition be $\nu_0 = (E_J - E_{J-1})/h$ then we find

$$\nu^0_M = \nu_0 + \mu_X B M (g_J - g_{J-1})/h, \tag{55}$$

noting that, for a π-transition, the frequency reverts to that of the unsplit transition if either $M = 0$ (the 'central π-transition') or if the Landé factors of the two rotational levels are equal. In this latter case, the frequencies of all the π-transitions are the same, resulting in a single π-spectral line centered on ν_0. The frequencies of the σ-transitions may be constructed in a similar manner, and the equation analogous to eq.(55), summarizing both types, is

$$\nu^{\pm}_M = \nu_0 + \mu_X B [M(g_J - g_{J-1}) \mp g_{J-1}]/h, \tag{56}$$

where the upper (lower) optional signs refer to σ^+ (σ^-) transitions. Note that a single frequency for each type again results, regardless of M, if both Landé factors are equal.

2.7.2 *Dipole Orientation*

The aim of this section is to relate the helical type of a magnetically-split transition to a particular spherical basis vector in the primed (magnetic field based) frame. The external magnetic field exerts a torque on the magnetic moment, equal to

$$\boldsymbol{\tau} = \boldsymbol{m} \times \boldsymbol{B} = -\mu_X g_J \boldsymbol{J} \times \boldsymbol{B} \tag{57}$$

(Enge et al. 1974). The second form on the right-hand side of eq.(57) results from elimination of the magnetic moment with the aid of eq.(50). With the aid of a diagram, Fig. 4, we can see that the torque is generally anticlockwise from the point of view of an IAU receiver-based observer (see Fig. 1), and therefore right-handed in the IEEE convention. As we are in the magnetic field (primed) frame, we can now say that the torque, and therefore the precessional motion of $\boldsymbol{J}$, is proportional to the right-handed spherical unit vector $\hat{\boldsymbol{e}}'_R$. A supporting analysis is given in Littlefield & Thorley (1979).

Having established that the direction of the precession of $\boldsymbol{J}$ about $\boldsymbol{B}$ (or the z' axis) is IEEE-right-handed, it is time to introduce the effect of transitions. For the sake of example, we shall consider a σ^+ transition, in fact the one marked by the red emission arrow in Fig. 3. M is the quantum number for the projection of $\boldsymbol{J}$ on the z' axis, and this has increased by one unit in transition: that is, a σ^+ transition in emission adds one unit of IEEE right-handed angular momentum about the z' axis to the molecule. Since

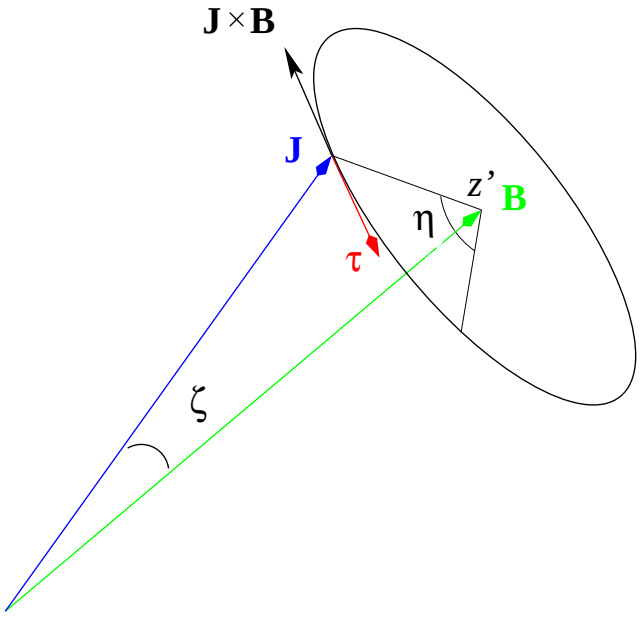

Figure 4. The torque on the molecular angular momentum vector due to a magnetic field along the z' axis: the vector cross product $\boldsymbol{J} \times \boldsymbol{B}$ points tangentially in the direction shown by definition. The magnitude of $\boldsymbol{J}$ and the angle ζ it makes to the magnetic field must remain constant in the absence of transition, so the head of the vector $\boldsymbol{J}$ moves in a circle, shown in projection as an ellipse, around the magnetic field. The torque exerted on $\boldsymbol{J}$, shown in red, is opposite in direction to the cross product from eq.(57). As the torque would still be tangential after advancing the head of $\boldsymbol{J}$ through an angle η, the motion of $\boldsymbol{J}$ is generally anticlockwise as viewed by an observer 'receiving' the magnetic field, and therefore described by the spherical vector $\hat{\boldsymbol{e}}'_R$ under the IEEE convention.

the transition is mediated by the electric dipole of the molecule, the dipole matrix element for a σ^+ transition in emission is also IEEE right-handed. This discussion is summarized and extended to stimulated emission in Green et al. (2014). Angular momentum about z' is conserved by the emission of an IEEE left-handed photon in the direction of increasing z', that is towards the observer. This conclusion is in agreement with the classical Lorentzian results, backed up by over 100 years of laboratory experiments, going back to the days of Zeeman himself. We have a magnetic field pointing towards the observer (Fig. 4), and the σ transition with the lower frequency (the σ^+) will be observed as emitting IEEE left-hand circularly polarized radiation (or the σ transition with the higher frequency (σ^-) will be observed emitting IEEE right-hand circularly polarized radiation.

In Section 2.3.1, we introduced the dipole matrix element for a transition between upper level p and lower level q as $\hat{\boldsymbol{d}}_{pq}$. We now need to replace this very general notation with something more applicable to the Zeeman group structure depicted in Figure 3. Our upper level can be identified by the quantum numbers (J, M), while the three possible options for the lower level are $(J', M+1)$ for σ^+, (J', M) for π or $(J', M-1)$ for σ^- transitions. Now we have shown above that, for the σ^+ transition type, the dipole is right-handed in the magnetic-field based (primed) axis system. For example,

$$\hat{\boldsymbol{d}}_{pq} = \hat{\boldsymbol{d}}_{(J,M),(J',M+1)} = \hat{d}_{(J,M),(J',M+1)}\hat{\boldsymbol{e}}'_R, \tag{58}$$

for a σ^+ dipole in the Zeeman group notation. By extension, the dipole of a σ^- transition is IEEE left-handed. It is well known that for radiation propagation parallel to the magnetic field, the π-transition does not appear. This means that the dipole has no component in the $x'y'$-plane, where it could interact with the electric field of the radiation, and must therefore lie along the z' axis. We may now write down three dipole definitions:

$$\sigma^+ : \hat{\boldsymbol{d}}_{pq} = \hat{\boldsymbol{d}}_{(J,M),(J',M+1)} = \hat{\boldsymbol{d}}^+_M = \hat{d}^+_M\hat{\boldsymbol{e}}'_R \tag{59a}$$

$$\pi : \hat{\boldsymbol{d}}_{pq} = \hat{\boldsymbol{d}}_{(J,M),(J',M)} = \hat{\boldsymbol{d}}^0_M = \hat{d}^0_M\hat{\boldsymbol{z}}' \tag{59b}$$

$$\sigma^- : \hat{\boldsymbol{d}}_{pq} = \hat{\boldsymbol{d}}_{(J,M),(J',M-1)} = \hat{\boldsymbol{d}}^-_M = \hat{d}^-_M\hat{\boldsymbol{e}}'_L, \tag{59c}$$

where the final forms introduce a useful shorthand that avoids the use of an excessive number of subscripts. It is unambiguous because: (i) all transitions are from J to J', and (ii) there is only one transition of each type leaving sublevel M in J. In the shorthand, the only subscript, M, still denotes the magnetic quantum number of the upper level, whilst the superscript indicates the change in M in emission.

2.7.3 Dipoles in the Radiation Frame

Having defined the dipoles as pure helical components in the primed frame (equation 59), we also derive a representation of the dipoles in the radiation-based (global, unprimed) frame. This is straightforwardly achieved by applying the rotation matrix, eq.(12), to the primed unit vectors in eq.(59), yielding

$$\begin{aligned}\hat{\boldsymbol{d}}^+_M &= \hat{d}^+_M[\hat{\boldsymbol{e}}_R(1+\cos\theta)(c-is)/2 \\ &\quad + \hat{\boldsymbol{z}}(i/\sqrt{2})\sin\theta + \hat{\boldsymbol{e}}_L(1-\cos\theta)(c+is)/2]\end{aligned} \tag{60a}$$

$$\begin{aligned}\hat{\boldsymbol{d}}^0_M &= (\hat{d}^0_M\sqrt{2})[\hat{\boldsymbol{e}}_R(s+ic)\sin\theta \\ &\quad + \sqrt{2}\hat{\boldsymbol{z}}\cos\theta + \hat{\boldsymbol{e}}_L(s-ic)\sin\theta]\end{aligned} \tag{60b}$$

$$\begin{aligned}\hat{\boldsymbol{d}}^-_M &= \hat{d}^-_M[\hat{\boldsymbol{e}}_R(1-\cos\theta)(c-is)/2 \\ &\quad - \hat{\boldsymbol{z}}(i/\sqrt{2})\sin\theta + \hat{\boldsymbol{e}}_L(1+\cos\theta)(c+is)/2],\end{aligned} \tag{60c}$$

where we have used the shorthand notation $c + is = \cos\phi' + i\sin\phi'$, and similar bracketed expressions. We also convert the dipole elements in eq.(60) to the Cartesian basis, using the definitions in eq.(9a) and eq.(9b) for the conversion:

$$\begin{aligned}\hat{\boldsymbol{d}}^+_M &= (\hat{d}^+_M/\sqrt{2})[\hat{\boldsymbol{x}}(\cos\phi' - i\cos\theta\sin\phi') \\ &\quad + \hat{\boldsymbol{y}}(\sin\phi' + i\cos\theta\cos\phi') + i\hat{\boldsymbol{z}}\sin\theta]\end{aligned} \tag{61a}$$

$$\hat{\boldsymbol{d}}^0_M = \hat{d}^0_M[\hat{\boldsymbol{x}}\sin\theta\sin\phi' - \hat{\boldsymbol{y}}\sin\theta\cos\phi' + \hat{\boldsymbol{z}}\cos\theta] \tag{61b}$$

$$\begin{aligned}\hat{\boldsymbol{d}}^-_M &= (\hat{d}^-_M/\sqrt{2})[\hat{\boldsymbol{x}}(\cos\phi' + i\cos\theta\sin\phi') \\ &\quad + \hat{\boldsymbol{y}}(\sin\phi' - i\cos\theta\cos\phi') - i\hat{\boldsymbol{z}}\sin\theta].\end{aligned} \tag{61c}$$

3 TIME-DOMAIN EQUATIONS

3.1 Interaction Hamiltonian

Elements of the interaction Hamiltonian have been previously introduced using the general transition pq in eq.(43), so the indices simply follow those of the matrix element of the dipole. We can therefore adopt the same shorthand notation for the elements relevant to our Zeeman group: $H^{\pm}_M$ for the $\sigma^{\pm}$ transitions and H^0_M for the π-transitions. In the σ^+ transition out of sub-level M, for example, the Hamiltonian element is $H^+_M = -\boldsymbol{E}\cdot\hat{\boldsymbol{d}}^+_M$. For the electric field, we take the real part of the Cartesian broad-band analytic signal, eq.(37). The results of the dot product with the three

forms of eq.(61) are,

$$H_M^+ = \{[(\tilde{\mathcal{E}}_R + \tilde{\mathcal{E}}_L)e^{-iY_0} + c.c.](\cos\phi' - i\sin\phi'\cos\theta) + [i(\tilde{\mathcal{E}}_R - \tilde{\mathcal{E}}_L)e^{-iY_0} + c.c.](\sin\phi' + i\cos\phi'\cos\theta + \sqrt{2}i[\tilde{\mathcal{E}}_z e^{-iY_0} + c.c.]\sin\theta\}(-d_M^+/4) \quad (62a)$$

$$H_M^0 = \{[[(\tilde{\mathcal{E}}_R + \tilde{\mathcal{E}}_L)e^{-iY_0} + c.c.]\sin\phi'\sin\theta - [i(\tilde{\mathcal{E}}_R - \tilde{\mathcal{E}}_L)e^{-iY_0} + c.c.]\cos\phi'\sin\theta + \sqrt{2}[\tilde{\mathcal{E}}_z e^{-iY_0} + c.c.]\cos\theta\}(-\sqrt{2}d_M^0/4) \quad (62b)$$

$$H_M^- = \{[(\tilde{\mathcal{E}}_R + \tilde{\mathcal{E}}_L)e^{-iY_0} + c.c.](\cos\phi' + i\sin\phi'\cos\theta) + [i(\tilde{\mathcal{E}}_R - \tilde{\mathcal{E}}_L)e^{-iY_0} + c.c.](\sin\phi' - i\cos\phi'\cos\theta) - \sqrt{2}i[\tilde{\mathcal{E}}_z e^{-iY_0} + c.c.]\sin\theta\}(-d_M^-/4) \quad (62c)$$

where $c.c.$ denotes the complex conjugate.

3.2 Off-Diagonal Equations

The Hamiltonian matrix elements in eq.(62) are specific to magnetic transition types, so we must develop sets of equations for the off-diagonal and diagonal DM elements that are similarly type-specific. Beginning with the off-diagonal DM elements that evolve according to eq.(44), we consider membership of the sum over j. We will assume that off-diagonal elements of the DM are negligible unless they correspond to an allowed electric dipole transition. This assumption is frequently, but not universally, made. Such elements are set to zero in Dinh-v-Trung (2009b), but Goldreich et al. (1973) make them constants in their analysis, whilst discussing the possibility that they may be comparable to those elements that correspond to the dipole transitions.

If, as we shall assume, the off-diagonal elements of the DM that correspond to forbidden electric dipole transitions are set to zero, an important simplification results: the sum over j in eq.(44) is empty for the Zeeman group introduced in Section 2.7.1 (Gray 2012). The result is that off-diagonal DM elements for all three transitions out of level (J, M) to magnetic sublevels in J' all evolve according to the generic equation,

$$D_t\rho_M = i\hat{H}_M\Delta_M/\hbar - (\gamma_M + i\omega_M)\rho_M \quad (63)$$

The off-diagonal elements of the DM have already been expanded as the product of a fast and a slow term in eq.(32), and we use this equation to eliminate ρ_M from eq.(63) in favour of the slowly-varying s_M. The result is

$$D_t s_M = -2\hat{H}_M\Delta_M e^{iY_0}/\hbar - [\gamma_M - i(\omega_0 - \omega_M - v\omega_0/c)]s_M. \quad (64)$$

We complete the derivation of type-dependent equations for the evolution of $s_M^\pm, s_M^0$ by introducing the appropriate forms of eq.(62) into eq.(64), and applying the rotating wave equation to remove terms oscillating rapidly at $e^{\pm iY_0}$. The evolution equations are,

$$D_t s_M^\pm = \frac{\Delta_M^\pm \hat{d}_M^\pm}{2\hbar}[(\tilde{\mathcal{E}}_R + \tilde{\mathcal{E}}_L)(c' \mp is'\cos\theta) + i(\tilde{\mathcal{E}}_R - \tilde{\mathcal{E}}_L)(s' \pm ic'\cos\theta) \pm \sqrt{2}i\tilde{\mathcal{E}}_z\sin\theta] - [\gamma_M^\pm + i(\Delta\omega_M^\pm + v\omega_0/c)]s_M^\pm \quad (65a)$$

$$D_t s_M^0 = \frac{\Delta_M^0 \hat{d}_M^0}{\sqrt{2}\hbar}[(\tilde{\mathcal{E}}_R + \tilde{\mathcal{E}}_L)s'\sin\theta - i(\tilde{\mathcal{E}}_R - \tilde{\mathcal{E}}_L)c'\sin\theta + \sqrt{2}\tilde{\mathcal{E}}_z\cos\theta] - [\gamma_M^0 + i(\Delta\omega_M^0 + v\omega_0/c)]s_M^0 \quad (65b)$$

where $c' = \cos\phi'$, $s' = \sin\phi'$, and the equations for both σ-transitions have been combined into the single equation, eq.(65a) with optional signs: the upper (lower) version of such signs refers to σ^+ (σ^-). Zeeman shifts are defined as

$$\Delta\omega_M^\pm = \mu_X B[M(g_J - g_{J1}) \mp g_{J1}]/\hbar \quad (66a)$$

$$\Delta\omega_M^0 = \mu_X BM(g_J - g_{J1})/\hbar, \quad (66b)$$

with the help of eq.(56) and eq.(55), respectively.

3.3 Inversion Equation

The sum in the equation for the evolution of the inversion, eq.(47), is not empty when we convert to the Zeeman group notation used in Section 3.2. Instead, they introduce interaction contributions from neighbouring transitions of all three polarization types, including those different from the type of the inversion in the differential. Membership of the sums is established in Gray (2012) and results in the following type-specific developments of eq.(47):

$$D_t\Delta_M^\pm = P_M^\pm\phi(v) - \Gamma_M^\pm\Delta_M^\pm - \frac{2}{\hbar}\Im\left\{2\rho_M^\pm\hat{H}_M^{\pm *} + \rho_M^0\hat{H}_M^{0*} + \rho_M^\mp\hat{H}_M^{\mp *} - \rho_{M+1}^{0*}\hat{H}_{M+1}^0 - \rho_{M+2}^{\mp *}\hat{H}_{M+2}^\mp\right\} \quad (67a)$$

$$D_t\Delta_M^0 = P_M^0\phi(v) - \Gamma_M^0\Delta_M^0 - \frac{2}{\hbar}\Im\left\{2\rho_M^0\hat{H}_M^{0*} + \rho_M^+\hat{H}_M^{+*} + \rho_M^-\hat{H}_M^{-*} - \rho_{M-1}^{+*}\hat{H}_{M-1}^+ - \rho_{M+1}^{-*}\hat{H}_{M+1}^-\right\}, \quad (67b)$$

where eq.(67a) refers to σ-transitions. The upper (lower) optional signs apply to σ^+ (σ^-). The case of π-transitions is covered by eq.(67b).

All of the interaction terms in eq.(67) may be written in the general form $\rho_x^a\hat{H}_x^{a*}$, or its complex conjugate, where $M - 2 \leqslant x \leqslant M + 2$ is an upper magnetic sublevel, and $a = 0, \pm$ is a transition type. The general interaction term may be developed by eliminating the Hamiltonian elements in favour of expressions from eq.(62), or complex conjugates thereof, and by using eq.(32), its conjugate, and the rotating wave approximation to remove all rapidly varying parts of the DM elements. We eventually obtain, for specific values of a,

$$\rho_x^\pm\hat{H}_x^{\pm *} = i\hat{d}_x^{\pm *}s_x^\pm[(\tilde{\mathcal{E}}_R^* + \tilde{\mathcal{E}}_L^*)(c' \pm is'\cos\theta) - i(\tilde{\mathcal{E}}_R^* - \tilde{\mathcal{E}}_L^*)(s' \mp ic'\cos\theta) \mp \sqrt{2}i\tilde{\mathcal{E}}_z^*\sin\theta]/8 \quad (68a)$$

$$\rho_x^0\hat{H}_x^{0*} = \sqrt{2}i\hat{d}_x^{0*}s_x^0[(\tilde{\mathcal{E}}_R^* + \tilde{\mathcal{E}}_L^*)s'\sin\theta + i(\tilde{\mathcal{E}}_R^* - \tilde{\mathcal{E}}_L^*)c'\sin\theta + \sqrt{2}\tilde{\mathcal{E}}_z^*\cos\theta]/8. \quad (68b)$$

With appropriate choices for x, the various forms of eq.(68) may be used to eliminate the interaction terms from eq.(67). The resulting, rather cumbersome, expressions are the evolution equations for the inversion in the three different types of transition. For brevity, we again combine the expressions for σ transitions into a single equation, with the upper form of any optional sign referring to σ^+.

Inversions evolve according to

$$
\begin{aligned}
&D_t\Delta_M^{\pm} = P_M^{\pm}\phi(v) - \Gamma_M^{\pm}\Delta_M^{\pm} - \frac{1}{4\hbar}\Im\{\\
&\sqrt{2}is'\sin\theta[\hat{d}_M^{0*}s_M^0(\tilde{\mathcal{E}}_R^*+\tilde{\mathcal{E}}_L^*) + \hat{d}_{M\pm1}^{0}s_{M\pm1}^{0*}(\tilde{\mathcal{E}}_R+\tilde{\mathcal{E}}_L)]\\
&-\sqrt{2}c'\sin\theta[\hat{d}_M^{0*}s_M^0(\tilde{\mathcal{E}}_R^*-\tilde{\mathcal{E}}_L^*) - \hat{d}_{M\pm1}^{0}s_{M\pm1}^{0*}(\tilde{\mathcal{E}}_R-\tilde{\mathcal{E}}_L)]\\
&+2i\cos\theta[\hat{d}_M^{0*}s_M^0\tilde{\mathcal{E}}_z^* + \hat{d}_{M\pm1}^{0}s_{M\pm1}^{0*}\tilde{\mathcal{E}}_z]\\
&+ic'[(\hat{d}_M^{\pm*}s_M^{\pm}+\hat{d}_M^{\mp*}s_M^{\mp})(\tilde{\mathcal{E}}_R^*+\tilde{\mathcal{E}}_L^*)+\hat{d}_{M\pm2}^{\mp}s_{M\pm2}^{\mp*}(\tilde{\mathcal{E}}_R+\tilde{\mathcal{E}}_L)]\\
&+s'[(\hat{d}_M^{\pm*}s_M^{\pm}+\hat{d}_M^{\mp*}s_M^{\mp})(\tilde{\mathcal{E}}_R^*-\tilde{\mathcal{E}}_L^*)-\hat{d}_{M\pm2}^{\mp}s_{M\pm2}^{\mp*}(\tilde{\mathcal{E}}_R-\tilde{\mathcal{E}}_L)]\\
&\mp ic'\cos\theta[(\hat{d}_M^{\pm*}s_M^{\pm}-\hat{d}_M^{\mp*}s_M^{\mp})(\tilde{\mathcal{E}}_R^*-\tilde{\mathcal{E}}_L^*)-\hat{d}_{M\pm2}^{\mp}s_{M\pm2}^{\mp*}(\tilde{\mathcal{E}}_R-\tilde{\mathcal{E}}_L)]\\
&\mp s'\cos\theta[(\hat{d}_M^{\pm*}s_M^{\pm}-\hat{d}_M^{\mp*}s_M^{\mp})(\tilde{\mathcal{E}}_R^*+\tilde{\mathcal{E}}_L^*)-\hat{d}_{M\pm2}^{\mp}s_{M\pm2}^{\mp*}(\tilde{\mathcal{E}}_R+\tilde{\mathcal{E}}_L)]\\
&\pm\sqrt{2}\sin\theta[(\hat{d}_M^{\pm*}s_M^{\pm}-\hat{d}_M^{\mp*}s_M^{\mp})\tilde{\mathcal{E}}_z^*+\hat{d}_{M\pm2}^{\mp}s_{M\pm2}^{\mp*}\tilde{\mathcal{E}}_z]\}
\end{aligned}
\tag{69a}
$$

$$
\begin{aligned}
&D_t\Delta_M^{0} = P_M^{0}\phi(v) - \Gamma_M^{0}\Delta_M^{0} - \frac{1}{4\hbar}\Im\{\\
&2\sqrt{2}i\hat{d}_M^{0*}s_M^0[s'\sin\theta(\tilde{\mathcal{E}}_R^*+\tilde{\mathcal{E}}_L^*)+ic'\sin\theta(\tilde{\mathcal{E}}_R^*-\tilde{\mathcal{E}}_L^*)+\sqrt{2}\tilde{\mathcal{E}}_z^*\cos\theta]\\
&+ic'[(\hat{d}_M^{+*}s_M^{+}+\hat{d}_M^{-*}s_M^{-})(\tilde{\mathcal{E}}_R^*+\tilde{\mathcal{E}}_L^*)+(\hat{d}_{M-1}^{+}s_{M-1}^{+*}+\hat{d}_{M+1}^{-}s_{M+1}^{-*})(\tilde{\mathcal{E}}_R+\tilde{\mathcal{E}}_L)]\\
&+s'[(\hat{d}_M^{+*}s_M^{+}+\hat{d}_M^{-*}s_M^{-})(\tilde{\mathcal{E}}_R^*-\tilde{\mathcal{E}}_L^*)-(\hat{d}_{M-1}^{+}s_{M-1}^{+*}+\hat{d}_{M+1}^{-}s_{M+1}^{-*})(\tilde{\mathcal{E}}_R-\tilde{\mathcal{E}}_L)]\\
&-s'\cos\theta[(\hat{d}_M^{+*}s_M^{+}-\hat{d}_M^{-*}s_M^{-})(\tilde{\mathcal{E}}_R^*+\tilde{\mathcal{E}}_L^*)-(\hat{d}_{M-1}^{+}s_{M-1}^{+*}-\hat{d}_{M+1}^{-}s_{M+1}^{-*})(\tilde{\mathcal{E}}_R+\tilde{\mathcal{E}}_L)]\\
&-ic'\cos\theta[(\hat{d}_M^{+*}s_M^{+}-\hat{d}_M^{-*}s_M^{-})(\tilde{\mathcal{E}}_R^*-\tilde{\mathcal{E}}_L^*)+(\hat{d}_{M-1}^{+}s_{M-1}^{+*}-\hat{d}_{M+1}^{-}s_{M+1}^{-*})(\tilde{\mathcal{E}}_R-\tilde{\mathcal{E}}_L)]\\
&+\sqrt{2}\sin\theta[(\hat{d}_M^{+*}s_M^{+}-\hat{d}_M^{-*}s_M^{-})\tilde{\mathcal{E}}_z^*-(\hat{d}_{M-1}^{+}s_{M-1}^{+*}-\hat{d}_{M+1}^{-}s_{M+1}^{-*})\tilde{\mathcal{E}}_z^*]\}
\end{aligned}
\tag{69b}
$$

3.4 Radiative Transfer Equations

In converting the general multi-level radiative transfer equation, eq.(34) to forms specific to the propagation of a Zeeman group, two problems need to br overcome: the membership of the sums, and the representation of the dipole elements in the radiation-based coordinates.

The outer sum is over upper energy levels. We may immediately discard all the levels in J' in our Zeeman group, since any downward electric dipole-allowed transition must begin in J (see Fig. 3). The outer sum therefore encompasses the sub-levels of J: it is over M from $-J$ to $+J$. The inner sum is over the lower levels of the electric dipole transitions, and is therefore immediately limited to the sub-levels of J'. However, again with reference to Fig. 3, we can see that for a given M in J there are at most three possible lower levels, each corresponding to a transition of different helical type because of the selection rule $\Delta M = 0, \pm 1$. Assuming that all of these transitions exist for a given M, we write the inner sum explicitly, so exchanging the order of summation and (velocity) integration we obtain from eq.(34) the Zeeman group transfer equation,

$$
d_t\tilde{\mathcal{E}}_q = \frac{\omega_0}{2\epsilon_0}\int_{-\infty}^{\infty} dv \sum_{M=-J}^{J} (\hat{d}_{M,q}^{+*}s_M^{+} + \hat{d}_{M,q}^{0*}s_M^{0} + \hat{d}_{M,q}^{-*}s_M^{-}). \tag{70}
$$

where $q = R, L, z$, and functional dependencies have been suppressed for brevity.

To address the second problem, we need a representation of the dipole vectors of the three transition types in components based on the global axis system. We already have this: eq.(59), but we need to take the complex conjugate to match all the dipole components in eq.(70). Noting that the spherical vectors used in eq.(9) have the property $\hat{\boldsymbol{e}}_R = \hat{\boldsymbol{e}}_L^*$ and $\hat{\boldsymbol{e}}_L = \hat{\boldsymbol{e}}_R^*$, the correct substitutions can be identified for all three values of q, and generating three versions of eq.(70):

$$
\begin{aligned}
d_t\tilde{\mathcal{E}}_R = \frac{\omega_0}{4\epsilon_0}\int_{-\infty}^{\infty} dv \sum_{M=-J}^{J} &\{\hat{d}_M^{+*}s_M^{+}(1-\cos\theta)(c'-is')\\
&+\sqrt{2}\hat{d}_M^{0*}s_M^0\sin\theta(s'+ic') + \hat{d}_M^{-*}s_M^{-}(1+\cos\theta)(c'-is')\}
\end{aligned}
\tag{71a}
$$

$$
\begin{aligned}
d_t\tilde{\mathcal{E}}_L = \frac{\omega_0}{4\epsilon_0}\int_{-\infty}^{\infty} dv \sum_{M=-J}^{J} &\{\hat{d}_M^{+*}s_M^{+}(1+\cos\theta)(c'+is')\\
&+\sqrt{2}\hat{d}_M^{0*}s_M^0\sin\theta(s'-ic') + \hat{d}_M^{-*}s_M^{-}(1-\cos\theta)(c'+is')\}
\end{aligned}
\tag{71b}
$$

$$
\begin{aligned}
d_t\tilde{\mathcal{E}}_z = \frac{\omega_0}{4\epsilon_0}\int_{-\infty}^{\infty} dv \sum_{M=-J}^{J} &\{\hat{d}_M^{+*}s_M^{+}(-\sqrt{2}i\sin\theta)\\
&+2\hat{d}_M^{0*}s_M^0\cos\theta + \hat{d}_M^{-*}s_M^{-}(\sqrt{2}i\sin\theta)\}
\end{aligned}
\tag{71c}
$$

The groups of equations, eq.(65), eq.(69) and eq.(71) now form a complete set of governing equations for the solution of the OAM maser problem with full polarization in the time domain. A reduction of the maser governing equations to the more standard Zeeman system with polarized radiation, but no OAM, may be effected by setting $c' = 1$, $s' = 0$ and $\tilde{\mathcal{E}}_z = 0$ in all these equations.

4 FREQUENCY-DOMAIN EQUATIONS

The easiest of the governing equations to transform to the frequency domain are the radiative transfer equations, because they are linear in the electric field amplitudes and DM elements. We use eq.(24) to write the time-domain quantities as transforms of the frequency-domain versions. After differentiation of the transform expression on the left-hand side, only a z-derivative remains, so that a set of PDEs in the time domain has been reduced to ODEs in frequency (Menegozzi & Lamb 1978; Dinh-v-Trung 2009b). Formal inverse transformation via eq.(25) then results in,

$$
\begin{aligned}
\frac{d\tilde{\mathcal{E}}_{R,n}}{dz} = \frac{\omega_0}{4c\epsilon_0}\int_{-\infty}^{\infty} dv \sum_{M=-J}^{J} &\{\hat{d}_M^{+*}s_{M,n}^{+}(1-\cos\theta)(c'-is')\\
&+\sqrt{2}\hat{d}_M^{0*}s_{M,n}^0\sin\theta(s'+ic') + \hat{d}_M^{-*}s_{M,n}^{-}(1+\cos\theta)(c'-is')\}
\end{aligned}
\tag{72a}
$$

$$
\begin{aligned}
\frac{d\tilde{\mathcal{E}}_{L,n}}{dz} = \frac{\omega_0}{4\epsilon_0}\int_{-\infty}^{\infty} dv \sum_{M=-J}^{J} &\{\hat{d}_M^{+*}s_{M,n}^{+}(1+\cos\theta)(c'+is')\\
&+\sqrt{2}\hat{d}_M^{0*}s_{M,n}^0\sin\theta(s'-ic') + \hat{d}_M^{-*}s_{M,n}^{-}(1-\cos\theta)(c'+is')\}
\end{aligned}
\tag{72b}
$$

$$
\begin{aligned}
\frac{d\tilde{\mathcal{E}}_{z,n}}{dz} = \frac{\omega_0}{4\epsilon_0}\int_{-\infty}^{\infty} dv \sum_{M=-J}^{J} &\{\hat{d}_M^{+*}s_{M,n}^{+}(-\sqrt{2}i\sin\theta)\\
&+2\hat{d}_M^{0*}s_{M,n}^0\cos\theta + \hat{d}_M^{-*}s_{M,n}^{-}(\sqrt{2}i\sin\theta)\}
\end{aligned}
\tag{72c}
$$

where we have introduced the following shorthand notations for the Fourier components:

$$
\tilde{\mathcal{E}}_{q,n} = \tilde{\mathcal{E}}_q(r,\phi,z,\varpi_n) \tag{73a}
$$

$$
s_{M,n} = s_M(r,\phi,z,\varpi_n,v) \tag{73b}
$$

$$
\Delta_{M,n} = \Delta_M(r,\phi,z,\varpi_n,v). \tag{73c}
$$

Transformation of eq.(65) is somewhat more difficult because of the appearance of products of inversions and electric field components on the right-hand sides. These products in the time domain will appear as convolutions in the frequency domain

(Menegozzi & Lamb 1978; Dinh-v-Trung 2009a). As an example, we write,

$$\tilde{\mathcal{E}}_R\Delta_M^+ = \mathcal{F}^{-1}[\tilde{\mathcal{E}}_{R,n}]\mathcal{F}^{-1}[\Delta_{M,n}^+] = \mathcal{F}^{-1}[\tilde{\mathcal{E}}_R \otimes \Delta_M^+]_{n-m}, \quad (74)$$

where the $\otimes$ symbol denotes the convolution operation. For a continuous frequency variable, the convolution would be an integral, but for the present system of finite-width Fourier components, we replace it with the sum,

$$[\tilde{\mathcal{E}}_R \otimes \Delta_M^+]_{n-m} = (2\pi)^{-1} \sum_{m=-\infty}^{\infty} \tilde{\mathcal{E}}_{R,m}\Delta_{M,n-m}^+, \quad (75)$$

and similar expressions for other polarizations and transition types. With the help of eq.(74) and eq.(75), and dropping terms of order v/c in size, the transformed versions of the evolution equations for off-diagonal elements of the DM become the algebraic equations:

$$s_{M,n}^{\pm} = \frac{\hat{d}_M^{\pm}\tilde{L}_M^{\pm}}{2\hbar} \sum_{m=-\infty}^{\infty} \Delta_{M,n-m}^{\pm}\{(1 \mp \cos\theta)(c' + is')\tilde{\mathcal{E}}_{R,m} + (1 \pm \cos\theta)(c' - is')\tilde{\mathcal{E}}_{L,m} \pm \sqrt{2}i\sin\theta\tilde{\mathcal{E}}_{z,m}\} \quad (76a)$$

$$s_{M,n}^{0} = \frac{\hat{d}_M^{0}\tilde{L}_M^{0}}{\sqrt{2}\hbar} \sum_{m=-\infty}^{\infty} \Delta_{M,n-m}^{0}\{\sin\theta(s' - ic')\tilde{\mathcal{E}}_{R,m} + \sin\theta(s' + ic')\tilde{\mathcal{E}}_{L,m} + \sqrt{2}\cos\theta\tilde{\mathcal{E}}_{z,m}\} \quad (76b)$$

where $\tilde{L}_M^{\pm}, \tilde{L}_M^0$ are the complex Lorentzian functions, defined by

$$\tilde{L}_M^{\pm,0} = \frac{1}{2\pi[\gamma^{\pm,0} - i(\varpi_n - \Delta\omega_M^{\pm,0} - v\omega_0/c)]}, \quad (77)$$

where the optional symbol $\pm, 0$ as a superscript encompasses all three transition types. The normalised real Lorentzian is, with the constant of 2π as used in eq.(77),

$$L_M^{\pm,0} = \tilde{L}_M^{\pm,0} + \tilde{L}_M^{(\pm,0)*} = \frac{\gamma_M^{\pm,0}/\pi}{(\gamma_M^{\pm,0})^2 + (\varpi_n - \Delta\omega_M^{\pm,0} - v\omega_0/c)^2}. \quad (78)$$

It is also necessary to transform the inversion equation, eq.(69), and this also contains time-domain products that will transform to frequency-domain convolutions. In this case, the products are all of electric field complex amplitudes with off-diagonal DM elements. Operations on the left-hand side proceed in a similar manner to those for the off-diagonal elements of the DM: terms of order v/c in the Doppler velocity are ignored, and the transformd equations are algebraic. On the right-hand side, there are two complicating issues: the first is the pumping term that is not a function of time. We write this as $P_M^+\phi(v)\mathcal{F}^{-1}[\delta_n]$, where we have taken the σ^+ version of eq.(69a) as an example, and δ_n is a δ-function that has the value 1 for $n = 0$ and zero for any other Fourier component. The second complication is that we must now transform complex conjugate quantities. We assume here that the discrete-width transforms used here follow the usual rules, that is for example,

$$\tilde{\mathcal{E}}_R^*(t) = (\mathcal{F}^{-1}[\tilde{\mathcal{E}}_{R,n}])^* = \mathcal{F}^{-1}[\tilde{\mathcal{E}}_{R,-n}^*]. \quad (79)$$

The products that will transform to convolutions are either of a conjugate complex amplitude and an ordinary off-diagonal DM element or vice-versa, resulting in the discrete representations,

$$\mathcal{F}^{-1}[\tilde{\mathcal{E}}_{R,n}]\mathcal{F}^{-1}[s_{M+1,-n}^{0*}] = \mathcal{F}^{-1}[\tilde{\mathcal{E}}_R \otimes s_{M+1}^{0*}]_{n-m} = (2\pi)^{-1} \sum_{m=-\infty}^{\infty} \tilde{\mathcal{E}}_{R,m}s_{M+1,m-n}^{0*} \quad (80a)$$

$$\mathcal{F}^{-1}[\tilde{\mathcal{E}}_{R,-n}^*]\mathcal{F}^{-1}[s_{M+1,n}^{0}] = \mathcal{F}^{-1}[\tilde{\mathcal{E}}_R^* \otimes s_{M+1}^{0}]_{n+m} = (2\pi)^{-1} \sum_{m=-\infty}^{\infty} \tilde{\mathcal{E}}_{R,m}^*s_{M+1,m+n}^{0}, \quad (80b)$$

and similarly for other transition types and polarizations. The resulting expressions for the inversions are

$$\begin{aligned}
\Delta_{M,n}^{\pm} &= P_M^{\pm}\phi(v)\delta_n/\Gamma_M^{\pm} - \tilde{\mathcal{L}}_M^{\pm}/(2\hbar) \sum_{m=-\infty}^{\infty} \{ \\
&\frac{\sin\theta}{\sqrt{2}}[(is' - c')(\hat{d}_M^{0*}s_{M,m+n}^{0}\tilde{\mathcal{E}}_{R,m}^* + \hat{d}_{M\pm1}^{0}s_{M\pm1,m-n}^{0*}\tilde{\mathcal{E}}_{L,m}) \\
&+ (is' + c')(\hat{d}_M^{0*}s_{M,m+n}^{0}\tilde{\mathcal{E}}_{L,m}^* + \hat{d}_{M\pm1}^{0}s_{M\pm1,m-n}^{0*}\tilde{\mathcal{E}}_{R,m}) \\
&\pm 2\hat{d}_M^{\pm*}s_{M,m+n}^{\pm}\tilde{\mathcal{E}}_{z,m}^* - \hat{d}_M^{\mp*}s_{M,m+n}^{\mp}\tilde{\mathcal{E}}_{z,m}^* + \hat{d}_{M\pm2}^{\mp*}s_{M\pm2,m-n}^{\mp*}\tilde{\mathcal{E}}_{z,m}] \\
&+ \frac{(1 \pm \cos\theta)}{2}[(s' + ic')(\hat{d}_M^{\mp*}s_{M,m+n}^{\mp}\tilde{\mathcal{E}}_{R,m}^*) \\
&- (s' - ic')(2\hat{d}_M^{\pm*}s_{M,m+n}^{\pm}\tilde{\mathcal{E}}_{L,m}^* + \hat{d}_{M\pm2}^{\mp*}s_{M\pm2,m-n}^{\mp*}\tilde{\mathcal{E}}_{R,m})] \\
&+ \frac{(1 \mp \cos\theta)}{2}[-(s' - ic')(\hat{d}_M^{\mp*}s_{M,m+n}^{\mp}\tilde{\mathcal{E}}_{L,m}^*) \\
&+ (s' + ic')(2\hat{d}_M^{\pm*}s_{M,m+n}^{\pm}\tilde{\mathcal{E}}_{R,m}^* + \hat{d}_{M\pm2}^{\mp}s_{M\pm2,m-n}^{\mp*}\tilde{\mathcal{E}}_{L,m})] \\
&+ i\cos\theta[\hat{d}_M^{0*}s_{M,m+n}^{0}\tilde{\mathcal{E}}_{z,m}^* + \hat{d}_{M\pm1}^{0}s_{M\pm1,m-n}^{0*}\tilde{\mathcal{E}}_{z,m}]\} \quad (81a)
\end{aligned}$$

$$\begin{aligned}
\Delta_{M,n}^{0} &= P_M^{0}\phi(v)\delta_n/\Gamma_M^{0} - \tilde{\mathcal{L}}_M^{0}/(2\hbar) \sum_{m=-\infty}^{\infty} \{ \\
&\frac{\sin\theta}{\sqrt{2}}[2\hat{d}_M^{0*}s_{M,m+n}^{0}((is' - c')\tilde{\mathcal{E}}_{R,m}^* + (is' + c')\tilde{\mathcal{E}}_{L,m}^*) \\
&+ (\hat{d}_M^{+*}s_{M,m+n}^{+} - \hat{d}_M^{-*}s_{M,m+n}^{-})\tilde{\mathcal{E}}_{z,m}^* \\
&- (\hat{d}_{M-1}^{+}s_{M-1,m-n}^{+*} - \hat{d}_{M+1}^{-}s_{M+1,m-n}^{-*})\tilde{\mathcal{E}}_{z,m}] \\
&+ \frac{(1+\cos\theta)}{2}[(s'+ic')(\hat{d}_M^{-*}s_{M,m+n}^{-}\tilde{\mathcal{E}}_{R,m}^* + \hat{d}_{M-1}^{+}s_{M-1,m-n}^{+*}\tilde{\mathcal{E}}_{L,m}) \\
&- (s' - ic')(\hat{d}_M^{+*}s_{M,m+n}^{+}\tilde{\mathcal{E}}_{L,m}^* + \hat{d}_{M+1}^{-}s_{M+1,m-n}^{-*}\tilde{\mathcal{E}}_{R,m})] \\
&+ \frac{(1-\cos\theta)}{2}[(s'+ic')(\hat{d}_M^{+*}s_{M,m+n}^{+}\tilde{\mathcal{E}}_{R,m}^* + \hat{d}_{M+1}^{-}s_{M+1,m-n}^{-*}\tilde{\mathcal{E}}_{L,m}) \\
&- (s' - ic')(\hat{d}_M^{-*}s_{M,m+n}^{-}\tilde{\mathcal{E}}_{L,m}^* + \hat{d}_{M-1}^{+}s_{M-1,m-n}^{+*}\tilde{\mathcal{E}}_{R,m})] \\
&+ 2i\cos\theta\hat{d}_M^{0*}s_{M,m+n}^{0}\tilde{\mathcal{E}}_{z,m}^*, \quad (81b)
\end{aligned}$$

where optional signs have been used in eq.(81a) to allow this equation to be used for both σ^+ (upper sign) and σ^- (lower sign). The complex Lorentzian function $\tilde{\mathcal{L}}_M^{\pm,0}$ is defined as

$$\tilde{\mathcal{L}}_M^{\pm,0} = (2\pi)^{-1}[\Gamma_M^{\pm,0} - i\varpi_n]^{-1}. \quad (82)$$

The set of equations comprising the subsets eq.(72), eq.(76) and eq.(81) now form a closed set for the solution of the full maser amplification problem with full polarization plus OAM in the frequency domain. All processes of saturation, population pulsation and mode coupling, for example, are included. The only auxilliary equations required are the definitions of the molecular velocity distribution function, eq.(48), and the definitions of the Zeeman frequency shifts, eq.(66). Suitable boundary conditions are to inject radiation for all Fourier components at $z = 0$ with no polarization and no OAM. This amounts to setting all z-component complex amplitudes to zero, and setting the left- and right-handed complex

amplitudes to values appropriate for background noise with Gaussian statistics. A suitable prescription is to set each phase to an independent value drawn from a uniform distribution, and each real amplitude to an independent value drawn from a normal distribution.

Such complexity is not necessary to answer the question of whether a maser can amplify OAM. By analogy with polarization, we only need to know whether it can grow: ignore all the more subtle effects, including even saturation, and study growth of intensity-like variables.

5 CLASSICAL REDUCTION

To make a classical reduction of our system of frequency-domain governing equations, we make the following approximations: (i) different Fourier components of the radiation field remain uncorrelated for any degree of saturation; (ii) population is restricted to a single central Fourier component, numbered zero; (iii) radiation statistics remain Gaussian at all signal strengths; (iv) Lorentzian functions act effectively as δ-functions. Point (iii) allows all correlation expressions of electric field amplitudes to be reduced to correlations of orders 1 and 2 only.

Immediate effects of the above reductions include the collapse of the sums over m in eq.(76) to a single element with $m = n$. An important consequence is that only the central Fourier component of the population inversion is required for each transition type, that is $\Delta^{\pm,0}_{M,0}$, and similarly for the other subscripts from $M-2$ to $M+2$. This restriction on the inversion also leads to a collapse of the sum over m in eq.(81), but we do not need to consider this further because we are considering only unsaturated amplification. The radiative transfer equations are not immediately affected by the classical approximations.

5.1 Stokes and OAM Parameters

A vector of four Stokes parameters gives a complete description of polarized radiation, but is inadequate to address the additional complication of radiation with OAM. Since we are measuring the amount of OAM by the presence of a z-component of the electric field, it makes sense to define new parameters that measure both the overall intensity present in this z-component and the intensity of its interaction with the left- and right-handed polarizations. To this end, we define the OAM parameters,

$$J_n = \langle \mathcal{J}_n \rangle = \langle \tilde{\mathcal{E}}_{z,n} \tilde{\mathcal{E}}^*_{z,n} \rangle \tag{83a}$$

$$G_n = \langle \mathcal{G}_n \rangle = \langle \tilde{\mathcal{E}}_{z,n} \tilde{\mathcal{E}}^*_{R,n} + \tilde{\mathcal{E}}_{R,n} \tilde{\mathcal{E}}^*_{z,n} \rangle \tag{83b}$$

$$H_n = \langle \mathcal{H}_n \rangle = \langle \tilde{\mathcal{E}}_{z,n} \tilde{\mathcal{E}}^*_{L,n} + \tilde{\mathcal{E}}_{L,n} \tilde{\mathcal{E}}^*_{z,n} \rangle \tag{83c}$$

$$W_n = \langle \mathcal{W}_n \rangle = i\langle \tilde{\mathcal{E}}_{z,n} \tilde{\mathcal{E}}^*_{R,n} - \tilde{\mathcal{E}}_{R,n} \tilde{\mathcal{E}}^*_{z,n} \rangle \tag{83d}$$

$$X_n = \langle \mathcal{X}_n \rangle = i\langle \tilde{\mathcal{E}}_{z,n} \tilde{\mathcal{E}}^*_{L,n} - \tilde{\mathcal{E}}_{L,n} \tilde{\mathcal{E}}^*_{z,n} \rangle \tag{83e}$$

noting that, like the Stokes parameters, all these new parameters are real. The angle brackets denote an average over a good statistical number of realizations of the electric field. Each realization, in the present context, corresponds to an individual spectral sample of duration T (Menegozzi & Lamb 1978; Dinh-v-Trung 2009a). The first of these new parameters is a measure of the total intensity of OAM present, as measured from the intensity of the z-component of the electric field. The other four parameters are a measure of the interaction of the OAM with the conventional electric field components in the xy (or $r\phi$) plane. By summing the squares of eq.(83b)-eq.(83e), it is straightforward to show that these parameters satisfy the relation,

$$G_n^2 + H_n^2 + W_n^2 + X_n^2 = 2 I_n J_n. \tag{84}$$

We also maintain the definition of the Stokes parameters that is compatible with the IEEE convention on left- and right-handed polarization, the IAU axis system, and the IAU convention that defines positive Stokes-V as an excess of right-handed over left-handed polarization. Such a set is,

$$I_n = \langle \mathcal{I}_n \rangle = \langle \tilde{\mathcal{E}}_{R,n} \tilde{\mathcal{E}}^*_{R,n} + \tilde{\mathcal{E}}_{L,n} \tilde{\mathcal{E}}^*_{L,n} \rangle \tag{85a}$$

$$Q_n = \langle \mathcal{Q}_n \rangle = \langle \tilde{\mathcal{E}}_{R,n} \tilde{\mathcal{E}}^*_{L,n} + \tilde{\mathcal{E}}_{L,n} \tilde{\mathcal{E}}^*_{R,n} \rangle \tag{85b}$$

$$U_n = \langle \mathcal{U}_n \rangle = i\langle \tilde{\mathcal{E}}_{R,n} \tilde{\mathcal{E}}^*_{L,n} - \tilde{\mathcal{E}}_{L,n} \tilde{\mathcal{E}}^*_{R,n} \rangle \tag{85c}$$

$$V_n = \langle \mathcal{V}_n \rangle = \langle \tilde{\mathcal{E}}_{R,n} \tilde{\mathcal{E}}^*_{R,n} - \tilde{\mathcal{E}}_{L,n} \tilde{\mathcal{E}}^*_{L,n} \rangle. \tag{85d}$$

We note that these Stokes parameters, and the OAM parameters in eq.(83), should formally be multiplied by a constant that gives them units of specific intensity. However, as we will construct equations below, in Section 5.2, that are linear in the Stokes and OAM parameters, we omit this constant as it will cancel from both sides of each equation.

5.2 Intensity Equations

We construct equations for the transport of the OAM and Stokes parameters by differentiating the definitions in eq.(83) and eq.(85) with respect to z. For example, the unaveraged form of the parameter $\mathcal{G}_n$ from eq.(83b) gives us,

$$\frac{d\mathcal{G}_n}{dz} = \tilde{\mathcal{E}}_{z,n} \frac{d\tilde{\mathcal{E}}^*_{R,n}}{dz} + \tilde{\mathcal{E}}^*_{R,n} \frac{d\tilde{\mathcal{E}}_{z,n}}{dz} + \tilde{\mathcal{E}}_{R,n} \frac{\tilde{\mathcal{E}}^*_{z,n}}{dz} + \tilde{\mathcal{E}}^*_{z,n} \frac{\tilde{\mathcal{E}}_{R,n}}{dz}. \tag{86}$$

The right-hand sides may be constructed from eq.(72a), eq.(72c) and their complex conjugates. The equations contain various forms of off-diagonal DM element, but these can in turn be eliminated via eq.(76), noting that, in our classical approximation, $m = n$ is the only term in the sum, and all inversions revert to the central Fourier component. A final realization average of eq.(86) yields the power-spectrum form, G_n. The same method may also be employed for all the other Stokes and OAM parameters. The results are summarized in the following five transfer equations for the OAM parameters, as

defined in eq.(83)

$$\frac{dJ_n}{dz} = \frac{1}{8\epsilon_0\hbar}\sum_{M=-J}^{J}\Big\{2J_n(2D^0_{M,n} - \Pi_{M,n}\sin^2\theta) + \frac{\sin\theta}{\sqrt{2}}(R_{M,n} + \Pi_{M,n}\cos\theta)(s'G_n + c'W_n) + \frac{\sin\theta}{\sqrt{2}}(\Pi_{M,n}\cos\theta - R_{M,n})(s'H_n - c'X_n)\Big\} \tag{87a}$$

$$\frac{dG_n}{dz} = \frac{1}{8\epsilon_0\hbar}\sum_{M=-J}^{J}\Big\{G_n(T_{M,n} - \frac{1}{2}\Pi_{M,n}\sin^2\theta - R_{M,n}\cos\theta) + \frac{s'\sin\theta}{\sqrt{2}}(R_{M,n} + \Pi_{M,n}\cos\theta)(I_n + V_n + 2J_n) - \frac{\sin\theta}{\sqrt{2}}(R_{M,n} - \Pi_{M,n}\cos\theta)(s'Q_n - c'U_n) - \frac{\Pi_{M,n}\sin^2\theta}{2}(H_n\cos 2\phi' + X_n\sin 2\phi')\Big\} \tag{87b}$$

$$\frac{dH_n}{dz} = \frac{1}{8\epsilon_0\hbar}\sum_{M=-J}^{J}\Big\{H_n(T_{M,n} - \frac{1}{2}\Pi_{M,n}\sin^2\theta + R_{M,n}\cos\theta) + \frac{s'\sin\theta}{\sqrt{2}}(\Pi_{M,n}\cos\theta - R_{M,n})(I_n - V_n + 2J_n) + \frac{\sin\theta}{\sqrt{2}}(R_{M,n} + \Pi_{M,n}\cos\theta)(s'Q_n - c'U_n) - \frac{\Pi_{M,n}\sin^2\theta}{2}(G_n\cos 2\phi' - W_n\sin 2\phi')\Big\} \tag{87c}$$

$$\frac{dW_n}{dz} = \frac{1}{8\epsilon_0\hbar}\sum_{M=-J}^{J}\Big\{W_n(T_{M,n} - \frac{1}{2}\Pi_{M,n}\sin^2\theta - R_{M,n}\cos\theta) + \frac{c'\sin\theta}{\sqrt{2}}(R_{M,n} + \Pi_{M,n}\cos\theta)(I_n + V_n + 2J_n) + \frac{\sin\theta}{\sqrt{2}}(R_{M,n} - \Pi_{M,n}\cos\theta)(c'Q_n + s'U_n) - \frac{\Pi_{M,n}\sin^2\theta}{2}(X_n\cos 2\phi' - H_n\sin 2\phi')\Big\} \tag{87d}$$

$$\frac{dX_n}{dz} = \frac{1}{8\epsilon_0\hbar}\sum_{M=-J}^{J}\Big\{X_n(T_{M,n} - \frac{1}{2}\Pi_{M,n}\sin^2\theta + R_{M,n}\cos\theta) + \frac{c'\sin\theta}{\sqrt{2}}(R_{M,n} - \Pi_{M,n}\cos\theta)(I_n - V_n + 2J_n) + \frac{\sin\theta}{\sqrt{2}}(R_{M,n} + \Pi_{M,n}\cos\theta)(c'Q_n + s'U_n) - \frac{\Pi_{M,n}\sin^2\theta}{2}(W_n\cos 2\phi' + G_n\sin 2\phi')\Big\}, \tag{87e}$$

and in the four following transfer equations for the Stokes parameters, as defined in eq.(85), noting that these and the five parts of eq.(83) together form a coupled set of nine ODEs.

$$\frac{dI_n}{dz} = \frac{1}{8\epsilon_0\hbar}\sum_{M=-J}^{J}\Big\{2I_n(D^+_{M,n} + D^-_{M,n}) - 2R_{M,n}V_n\cos\theta + \Pi_{M,n}(I_n - Q_n\cos 2\phi' - U_n\sin 2\phi')\sin^2\theta + \frac{\sin\theta}{\sqrt{2}}(R_{M,n} + \Pi_{M,n}\cos\theta)(s'G_n + c'W_n) - \frac{\sin\theta}{\sqrt{2}}(R_{M,n} - \Pi_{M,n}\cos\theta)(s'H_n - c'X_n)\Big\} \tag{88a}$$

$$\frac{dV_n}{dz} = \frac{1}{8\epsilon_0\hbar}\sum_{M=-J}^{J}\Big\{[2(D^+_{M,n} + D^-_{M,n}) + \Pi_{M,n}\sin^2\theta]V_n - 2R_{M,n}I_n\cos\theta + \frac{\sin\theta}{\sqrt{2}}(R_{M,n} - \Pi_{M,n}\cos\theta)(s'H_n - c'X_n) + \frac{\sin\theta}{\sqrt{2}}(R_{M,n} + \Pi_{M,n}\cos\theta)(s'G_n + c'W_n)\Big\} \tag{88b}$$

$$\frac{dQ_n}{dz} = \frac{1}{8\epsilon_0\hbar}\sum_{M=-J}^{J}\Big\{[2(D^+_{M,n} + D^-_{M,n}) + \Pi_{M,n}\sin^2\theta]Q_n + [c'(W_n + X_n) - s'(G_n - H_n)]\frac{\sin\theta}{\sqrt{2}}(R_{M,n} - \Pi_{M,n}\cos\theta) - \Pi_{M,n}I_n\sin^2\theta\cos 2\phi'\Big\} \tag{88c}$$

$$\frac{dU_n}{dz} = \frac{1}{8\epsilon_0\hbar}\sum_{M=-J}^{J}\Big\{[2(D^+_{M,n} + D^-_{M,n}) + \Pi_{M,n}\sin^2\theta]U_n + [c'(G_n - H_n) + s'(W_n + X_n)]\frac{\sin\theta}{\sqrt{2}}(R_{M,n} - \Pi_{M,n}\cos\theta) - \Pi_{M,n}I_n\sin^2\theta\sin 2\phi'\Big\}. \tag{88d}$$

In deriving the set of equations, eq.(87), we have defined the following variables related to the inversions:

$$\Pi_{M,n} = 2D^0_{M,n} - D^+_{M,n} - D^-_{M,n} \tag{89a}$$

$$R_{M,n} = D^+_{M,n} - D^-_{M,n} \tag{89b}$$

$$T_{M,n} = 2D^0_{M,n} + D^+_{M,n} + D^-_{M,n} \tag{89c}$$

The first of these variables, $\Pi_{M,n}$, represents any dominance of the inversion in the π-transition over the summed inversions in both σ-transitions at a frequency local to Fourier component n. The second variable, $R_{M,n}$, expresses any imbalance in the inversions of the σ-transitions at the same frequency. This imbalance will be large in a Zeeman group such as those found in typical OH masers where, in a magnetic field of a few mG, the σ^+ and $\sigma-$ spectral lines propagate effectively independently.

The inversion-related functions $D^{\pm,0}_{M,n}$ are defined in general through the velocity integrals,

$$D^{\pm,0}_{M,n} = (\omega_0/c)|\hat{d}^{\pm,0}_M|^2\left\langle\int_{-\infty}^{\infty}\Delta^{\pm,0}_{M,0}(v)L^{\pm,0}_M(v)dv\right\rangle, \tag{90}$$

where the spatial functional dependence of the inversion has been omitted. The factor of ω_0/c is included because the Lorentzian, as defined in eq.(78), is normalized in frequency, and this extra factor is required to normalize it in velocity. In the specific case of negligible saturation, all terms in the radiation complex amplitudes may be dropped from eq.(81), so that, in all three versions, the inversion in Fourier component zero reduces to the combined form,

$$\Delta^{\pm,0}_{M,0}(v) = P^{\pm,0}_M\phi(v)/\Gamma^{\pm,0}_M, \tag{91}$$

and, when this is substituted into eq.(90), the integration can be

carried out, on the assumption that the Lorentzian tends to a δ-function. The realization averaging can also be dropped, because eq.(91) contains no electric field amplitudes or elements of the DM. With these points noted,

$$D^{\pm,0}_{M,n} = (|\hat{d}^{\pm,0}_M|^2 P^{\pm,0}_M/\Gamma^{\pm,0}_M)\phi[(c/\omega_0)(\varpi_n - \Delta\omega^{\pm,0}_M)]. \quad (92)$$

Note that the Gaussian function is now in terms of local frequency, and peaks at the Zeeman-shifted response frequency of the relevant transition type.

6 DISCUSSION

Several useful points may be raised by considering various limits and special cases of eq.(87) and eq.(88). The first is that the parameter J_n is not directly coupled to any of the Stokes parameters, as may be seen from eq.(87a). As this parameter effectively represents the intensity of the z-component of the electric field, such intensity can only arise indirectly from the Stokes parameters via the other four OAM parameters that represent interactions of the z-component of the electric field with circularly-polarized amplitudes in the $x-y$ plane. However, eq.(87a) does contain a term in J_n on the right-hand side that allows it to amplify itself, even if it needs G_n, H_n, W_n and X_n and the Stokes parameters to grow from an initally zero background level.

The second main point is that any effect involving OAM, at least if we require it to grow from an OAM-free background, will be strongest when the magnetic field is close to perpendicular to the z-axis ($\sin\theta = 1$ or $\theta = \pi/2$). If we take this limit, then J_n remains coupled to G_n, H_n, W_n and X_n, whilst these latter four parameters remain coupled to all four Stokes parameters as well as to linear combinations of themselves with coefficients formed from certain trigonometric functions of ϕ'. The equations describing the evolution of the Stokes parameters retain a similar coupling to the OAM parameters, though not directly to J_n as discussed above. By contrast, in the other limit, where the magnetic field lies parallel to the z-axis, most of the above couplings are eliminated: the Stokes parameters couple only to themselves and combinations of other Stokes parameters. All five OAM parameters are left with the capacity only to amplify themselves, so no OAM at all can result from an OAM-free background in the parallel configuration.

A third important point, when considering the case where $\sin\theta = 1$, is that all the terms that couple Stokes parameters to OAM parameters include a factor of $R_{M,n}$. From eq.(89b), we can see that this parameter is essentially the difference between the inversions in the σ^+ and σ^- transitions. Unless we have a pumping process that is asymmetric, favouring one of these over the other (say $P^+_M > P^-_M$), then we will obtain a number very close to zero for typical closed shell maser molecules, such as water, methanol and SiO, where the Zeeman splitting is likely to be dwarfed by the inhomogeneous (Doppler) line width. The most likely source of OAM is therefore in OH (and possibly CH) masers, where the Zeeman splitting may comfortably exceed the Doppler width. In this case, if we choose a Fourier component, n, near the centre of the σ^+ line, we will find $R_{M,n} \simeq D^+_{M,n}$, with almost no contamination from the σ^- line, even if the pumping is symmetric. The best possible situation for generating OAM in a maser, from an OAM-free background, is therefore in an open-shell molecule with a large Zeeman splitting, from a σ-type transition and a non-uniform magnetic field lying in the $x-y$ plane. Under these circumstances, the OAM parameters G_n, H_n, W_n and X_n can interact directly with Stokes-I and (independently) with J_n. Note that the terms that couple G_n, H_n, W_n and X_n to J_n also contain a comman factor of $R_{M,n}$ when $\theta = \pi/2$. Generation of OAM may offer a new explanation for the observation that linearly polarized Zeeman triplets, expected for a perpendicular magnetic field, are very rare or absent.

6.1 Restricted Solutions

Having made the general observations above, we now consider analytic solutions of eq.(87) and eq.(88) under a set of conditions that correspond to optimum generation of OAM: we take the magnetic field to be perpendicular to the line of sight ($\theta = \pi/2$), and pick a Fourier component, $n = k$, that corresponds to the line centre of the σ^+ line in a molecule and transition (for example the rotational ground state of OH) that has a Zeeman splitting that can easily exceed the Doppler line width. Under these conditions, we may make the reductions, $D^-_{M,k} = 0$, $R_{M,k} = T_{M,k} = D_{M,k}$ and $\Pi_{M,k} = -D_{M,k}$, so that $D^+_{M,k}$ becomes a common factor on the right-hand side of all the governing equations. We extract this factor, and use it to construct the dimensionless line-of-sight distance,

$$d\zeta = dz D^+_{M,k}/(8\epsilon_0\hbar). \quad (93)$$

We assume that the seed radiation of the maser is unpolarized and OAM-free, with Stokes-I intensity equal to I_{BG}. We divide all the governing equations by I_{BG}, and define dimensionless Stokes and OAM parameters as, for example, $i_k = I_k/I_{BG}$, $q_k = Q_k/I_{BG}$, and similarly for all the other parameters, writing lower-case letters for the dimensionless forms.

We consider the magnetic field to be of ideal quadrupole form, with Cartesian components given by $B_x = \boldsymbol{B}_0 \cdot \boldsymbol{y}$ and $B_y = \boldsymbol{B}_0 \cdot \boldsymbol{x}$, where $\boldsymbol{B}_0$ is a constant. We pick, for the sake of example, a point on the y-axis, where $\phi = \pi/2$. At this point, $B_y = 0$ and $B_x = B_0 y$, and from eq.(8), we recover $\phi' = \arccos(0) = \pi/2$. We may therefore insert into all the governing equations the special values, $\sin\phi' = s' = 1$, $\cos\phi' = c' = 0$, $\sin 2\phi' = 0$ and $\cos 2\phi' = -1$. When this has been done, then by inspection, the nine governing equations break into two decoupled sets: one set of three contains exclusively functions of q_k, w_k, x_k, whilst the other six equations are entirely free of these parameters. As all of q_k, w_k, x_k are zero at $z = \zeta = 0$, and are decoupled from i_k, the only parameter with a non-zero background, we discard the smaller set, and write down the remaining six equations:

$$dj_k/d\zeta = 2j_k + (g_k - h_k)/\sqrt{2} \quad (94a)$$

$$dg_k/d\zeta = (i_k + v_k + 2j_k - q_k)/\sqrt{2} + (3g_k - h_k)/2 \quad (94b)$$

$$dh_k/d\zeta = (v_k - i_k - 2j_k + q_k)/\sqrt{2} + (3h_k - g_k)/2 \quad (94c)$$

$$di_k/d\zeta = i_k - q_k + (g_k - h_k)/\sqrt{2} \quad (94d)$$

$$dq_k/d\zeta = q_k - i_k - (g_k - h_k)/\sqrt{2} \quad (94e)$$

$$dv_k/d\zeta = v_k + (g_k + h_k)/\sqrt{2}. \quad (94f)$$

The set of equations, eq.(94), are soluble analytically. The first step to a solution is to add eq.(94d) to eq.(94e): the right-hand side of the combined equation is zero, so that $i_k + q_k$ is a constant, and under our assumed background conditions,

$$i_k(\zeta) + q_k(\zeta) = 1. \quad (95)$$

A second useful summation is to add eq.(94b) to eq.(94c), and then to add the result to $\sqrt{2}$ times eq.(94f). The result is the differential

equation

$$d/d\zeta(\sqrt{2}v_k + g_k + h_k) = 2(\sqrt{2}v_k + g_k + h_k). \quad (96)$$

If we set $\sigma_k = \sqrt{2}v_k + g_k + h_k$, eq.(96) has the solution $\sigma(\zeta) = \sigma(0)e^{2\zeta}$, but since $\sigma(0) = 0$ under our background conditions, $\sigma(\zeta)$ is also zero for any larger distance. We therefore require that

$$g_k(\zeta) + h_k(\zeta) = -\sqrt{2}v_k(\zeta). \quad (97)$$

We use eq.(95) and eq.(97) to eliminate q_k and v_k from eq.(94). Subtraction of the resulting equation in h_k from its counterpart in g_k then yields

$$d/d\zeta(g_k - h_k) = 2\sqrt{2}[i_k + j_k + (g_k - h_k)/\sqrt{2} - 1/2], \quad (98)$$

and, as g_k and h_k appear only as the combination $g_k - h_k$ in the remaining equations, we may introduce the new variable $y_k = g_k - h_k$, and write the three remaining equations as

$$dj_k/d\zeta = 2j_k + y_k/\sqrt{2} \quad (99a)$$

$$dy_k/d\zeta = 2\sqrt{2}(i_k + j_k + y_k/\sqrt{2} - 1/2) \quad (99b)$$

$$di_k/d\zeta = 2i_k + y_k/\sqrt{2} - 1. \quad (99c)$$

We now let $f_k = i_k + j_k$, and add eq.(99a) to eq.(99c), leaving the pair of equations,

$$dy_k/d\zeta = 2\sqrt{2}(f_k + y_k/\sqrt{2} - 1/2) \quad (100a)$$

$$df_k/d\zeta = 2f_k + \sqrt{2}y_k - 1. \quad (100b)$$

Reduction to a single equation is achieved by multiplying eq.(100b) by $\sqrt{2}$ and adding the result to eq.(99b). If we define $l_k = y_k + \sqrt{2}f_k$, the final equation, in standard form as a first-order linear ODE, is

$$dl_k/d\zeta - 4l_k = -2\sqrt{2}. \quad (101)$$

Equation 101 may be solved by standard methods, and it is then strightforward to work back through the sequence of intermediate variables, and the constraints from eq.(95) and eq.(97) to the solution of eq.(94):

$$i_k(\zeta) = (e^{4\zeta} + 2e^{2\zeta} + 5)/8 \quad (102a)$$

$$j_k(\zeta) = (e^{4\zeta} - 2e^{2\zeta} + 1)/8 \quad (102b)$$

$$q_k(\zeta) = (3 - e^{4\zeta} - 2e^{2\zeta})/8 \quad (102c)$$

$$g_k(\zeta) = (e^{4\zeta} - 1)/(4\sqrt{2}), \quad (102d)$$

together with the subsidary relations, $h_k(\zeta) = -g_k(\zeta)$ and, consequently $v_k(\zeta) = 0$. By inspection of eq.(102), we can see that all the Stokes and OAM parameters at moderate signal strengths (much greater than background, but not saturating) tend to a rising exponential of the form $e^{4\zeta}$, so the OAM parameters are likely to follow the polarization parameters to achieve levels such that j_k/i_k and $g_k/(\sqrt{2}i_k)$ tend to 1. The functions are plotted in the small signal limit in Figure 5.

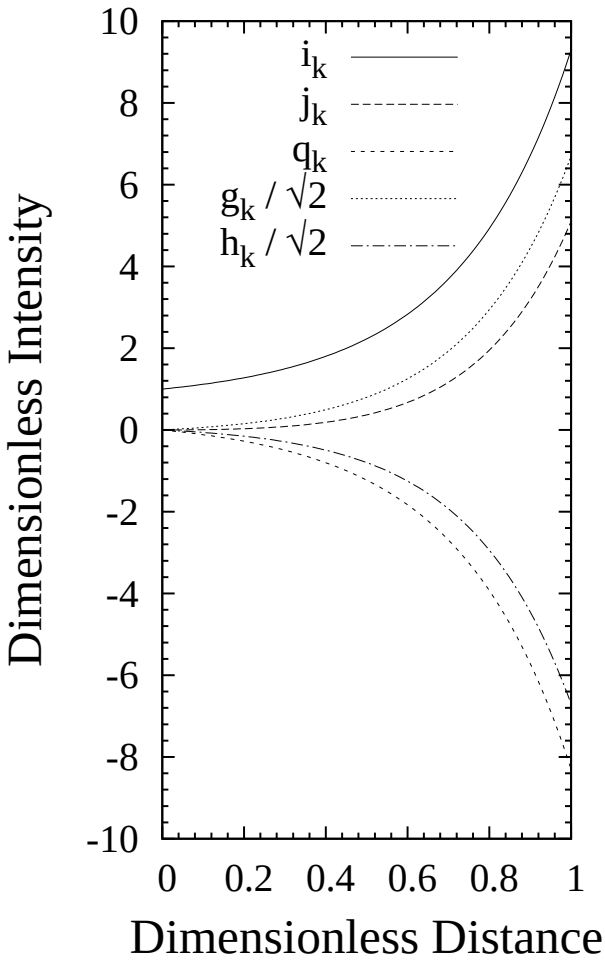

Figure 5. The non-zero dimensionless Stokes and OAM parameters as functions of dimensionless distance, ζ, in the small signal limit.

6.2 Numerical Experiment

The analytic solutions in Section 6.1 have demonstrated a non-trivial coupling of the z-component of the electric field to the conventional Stokes parameters. However, these results do not demonstrate a typical OAM pattern. In this section, we consider the same quadrupole magnetic field structure, but sample the field at many radii and azimuthal angles, ϕ. The analytical solutions above may be considered a single spatial sample from this array of points.

Additional geometrical considerations now need to be considered. The magnetic field magnitude now increases outwards from the origin, where it is zero and the overlap of the π and σ responses is complete. There will therefore be no polarization or OAM generated at the origin. As the radius is increased, the Zeeman splitting will rise, and the centre of the σ^+ response will move redward towards our chosen frequency, ϖ_k. As the radius continues to increase, ϖ_k will sample a decreasing wing of the Gaussian response. Although the magnetic field intensity continues to rise, the exponential drop in the response will ensure that, beyond a certain radius, there will be negligible amplification at ϖ_k. Rather arbitrarily, we will set ϖ_k to be -3 Doppler full widths ($k = -3$) to the red of the pattern line centre, ω_0. This value ensures a clean separation between the π and σ line shapes.

Our definition of ζ in this section differs slightly from that in Section 6.1. Here, we reduce eq.(88) and eq.(87) to dimensionless form by dividing all equations by the group $D_{0,0} = |d_0|^2 P_0 \phi(0)/\Gamma_0$: we have assumed $M = 0$ and symmetric pumping $P_M^+ = P_M^- = P_M^0 = P_0$, and similarly for the dipoles and loss-rates. As a consequence, dimensionless inversion expressions, such as $R_{0,k}$ and $\Pi_{0,k}$ reduce simply to differences of various Gaussians, centered on the associated molecular responses. For example,

$$R_{0,k} = e^{-[(\varpi_k - \Delta\omega_0^+)/\Delta\omega_D]^2} - e^{-[(\varpi_k - \Delta\omega_0^-)/\Delta\omega_D]^2}, \qquad (103)$$

where $\Delta\omega_D = w\omega_0/c$, and w is in turn defined in eq.(49). All radiation parameters are scaled by the level of the input seed radiation in Stokes-I; the other radiation parameters all have a background level of 0. The dimensionless evolution equations were solved using a Runge-Kutta fourth-order method with adaptive step-size control, maintained by a fifth-order accuracy checker (Press et al. 1992). The results discussed below were drawn from a run with an integration accuracy of 2×10^{-7}.

In Figure 6, we plot the emergent radiation parameters as a function of distance from the origin (position of zero magnetic field) on Cartesian axes. These axes conform to the IAU standard, as discussed in Section 2.1, so that the x-axis points vertically up the page (North) and the y-axis increases to the left. Distances are in magnetic field strength units, as required to yield a certain Zeeman splitting in Doppler widths. The azimuthal angle, ϕ is measured anticlockwise from its zero position at North. The z-axis, along which the radiation propagated, points out of the page towards the observer, and all parameters have been amplified over the same dimensionless distance of $\zeta = 4.0$, a value that corresponds to moderate amplification: peak values of Stokes-I are vastly greater than the background, but still low enough that saturation is negligible for a realistic OH maser that is amplifying a CMB background.

In all cases, the radial structure of the radiation pattern is controlled by a combination of the magnetic field strength (which increases outwards) and the Doppler response of the molecules, which may be considered Gaussian. We see the brightest emission close to a radius of 3, where the magnetically shifted response in the σ^+ part of the Zeeman pattern lies closest to our chosen Fourier component with $k = -3$. Different Fourier components will exhibit different patterns. Choosing $k = +3$ would produce a very similar radial pattern, but with the signs of some parameters reversed.

The angular distributions are determined partly by the angular functions of ϕ' that appear in eq.(87) and eq.(88) (variously sines and cosines of either ϕ' or $2\phi'$) and partly by the exponential nature of the maser amplification. In particular, all OAM parameters are zero, as are Stokes-U and V, at $\phi = \phi' = 0$, the standard reduction to the case of a uniform magnetic field. This confirms the hypothesis that OAM cannot be generated from a uniform field, an outcome that is not obvious by inspection of eq.(87).

A difference between Stokes-I and the OAM-J parameter that is not immediately apparent in Figure 6 is that I is not zero at $\phi = 0$: instead, it has a value of 1.45×10^3, compared to its peak of 1.05×10^6 at $\phi = \pi/2$ and $3\pi/2$. The maxima of I and J are very similar, indicating that the fractional level of OAM, like polarization, may become very large without invoking saturation. The only other parameter that is non-zero at $\phi = 0$ (and π) is Stokes-Q: it is *positive* at this angle, with a value of 1.45×10^3, before giving way to negative values of much larger magnitude at angles closer to the y-axis. Physically, the larger values of Stokes-I near $\phi = \pi/2$, compared to $\phi = 0$, probably result from the radiation at the former position coupling to all three Cartesian components of the molecular dipole; at the latter position, corresponding to the polarization-only case, radiation can couple only to the dipole components in the xy-plane.

There is a general hierarchy of (absolute) peak values: levels of approximately 10^6 are achieved by the Stokes parameters I and Q, by the z-component intensity, J, and the two symmetric coupling parameters G and H. A second set, comprising the asymmetric coupling parameters W and X, together with Stokes U, achieve peaks of order one order of magnitude lower $\sim 10^5$. Finally Stokes-V is very weakly amplified, always negative, and has an absolute peak of ~ 700. It is probably also worth noting that whilst non-zero values of W are exclusively positive, X it not completely negative, achieving a positive peak of approximately 680.

The exponential nature of maser amplification introduces a number of feaures that are not typical of radiation beams with OAM in the laboratory. For example, a laboratory beam in an L-G mode with azimuthal order $l = 2$ might be expected to have an annular intensity pattern, and a $\sin 2\phi$ structure in phase. It should be pointed out here that the intensity, as represented by Stokes-i in Figure 6, is annular, but amplified interaction with other Stokes and OAM parameters have introduced an additional very strong angular structure. Parameters more sensitive to the phase, such as G, H, W, X show a pattern that is close to $\sin\phi$ (for G,H) and $\sin 2\phi$ (in W and X) at low amplification, but these patterns again become distorted by exponential growth. Peaks in the weaker parameters, for example W and X, at odd multiples of $\pi/4$ migrate with amplification towards the peaks of the stronger parameters.

Lack of linearly polarized Zeeman triplet patterns is a well-known observational feature of OH maser sources. Such patterns would logically arise from the propagation of maser radiation perpendicular to magnetic field lines, but appear rare compared to the Zeeman pairs of opposite-handed circular or elliptically polarized components generated by propagation that is close to aligned with the magnetic field. Many reasons for the lack of triplets have been suggested, including MHD turbulence (Goldreich & Sridhar 1995), Faraday depolarization within the source (Goldreich et al. 1973) and preferential beaming along magnetic field lines (Gray & Field 1994). Another possibility, arising from the present work, is that linearly-polarized masers may also possess high degrees of OAM, and may therefore be invisible to conventional radio detection equipment. It is certainly most unlikely that magnetic fields perpendicular to the line of sight will be totally uniform, but they do seem to be ordered on the scale of the source, down to a clustering scale of order 70 AU. For an OAM scheme to work, magnetic fields would need to be non-uniform on the scale of individual VLBI maser spots: perhaps 10 AU or even less, and evidence that the sky-component of the magnetic field tends to be aligned with the long axis of an individual spot (Fish & Reid 2006) suggests some ordering of the field even at this scale. Nevertheless, while the arrangement used in the present work is highly idealized, a significant yield of radiation with OAM from at least some OH masers seems likely.

The radiation patterns produced as a function of radius and angle in the present work do not correspond to any single Laguerre-Gaussian mode. However, they do reveal the underlying symmetry of the magnetic field, and the spectrum of modes present is therefore likely to yield information about the structure of the magnetic field on scales smaller than the size of the maser spot itself. By contrast, polarization, assuming a uniform field in each spot, can only tell us about the variation of the magnetic field over an area of sky containing many spots. The fraction of radiation converted to OAM also helps us to reconstruct the magnetic field in 3-D, since a field parallel to the line of sight produces no OAM (if the background radiation has none), whilst increasing amounts of OAM result as θ is increased towards $\pi/2$.

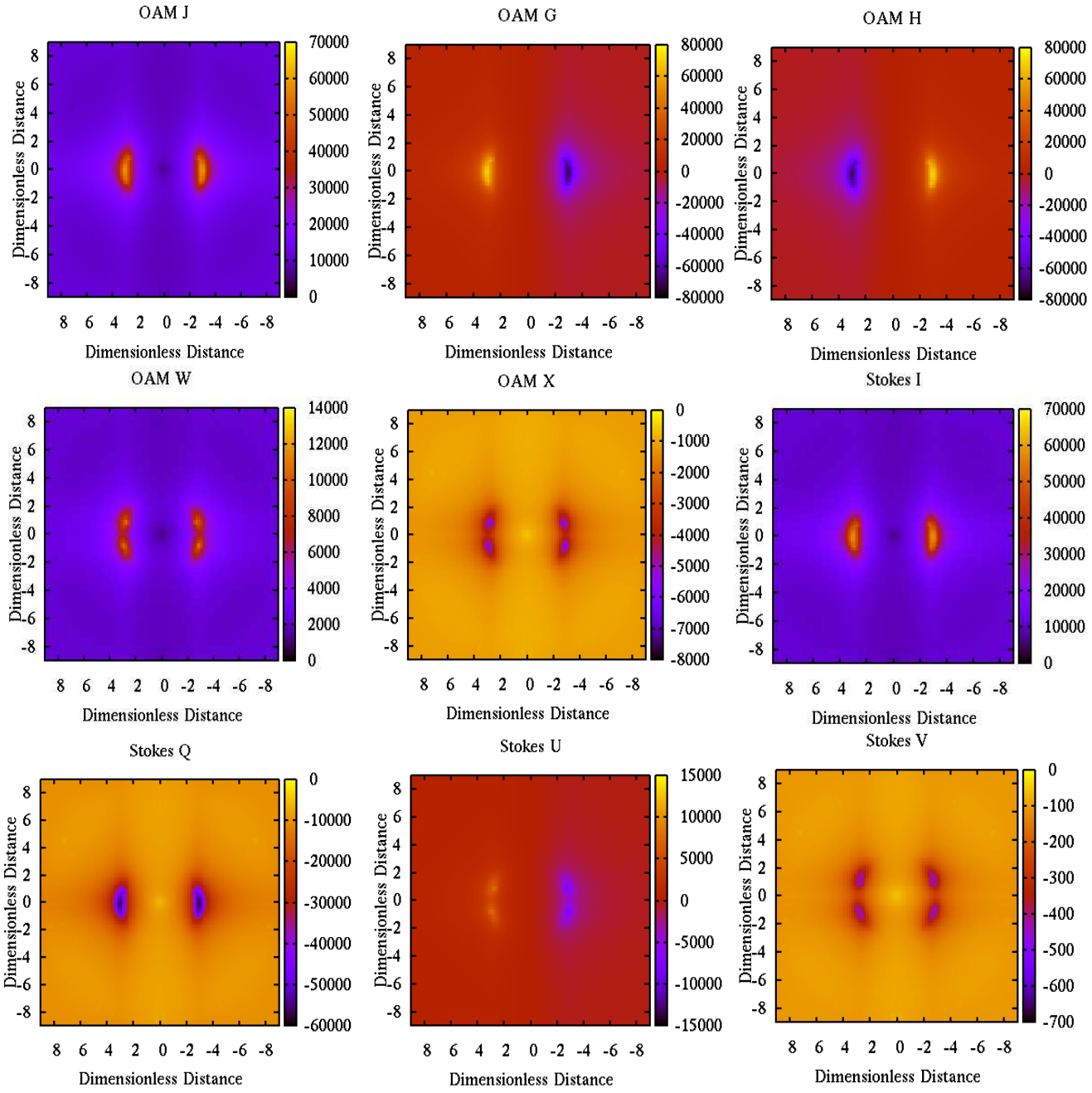

Figure 6. The emergent radiation parameters of a single Fourier component in the sky plane after propagation along the z-axis over a dimensionless distance of $\zeta = 4.0$. Each sub-figure has its own colour scale, shown to the right of the diagram. Figures on this scale are multiples of the seed value of Stokes-I. The x and y axes are drawn to conform to the IAU convention: with radiation approaching, x increases up the page, and y, to the left. The x and y axes are in Doppler or Zeeman units, so a distance of three units from the origin produces a magnetic field capable of shifting the response of a σ-transition by three Doppler widths from the frequency of the central π-component.

7 CONCLUSIONS

We have extended the standard theory of propagation of polarized astrophysical maser radiation to the case of a non-uniform magnetic field, allowing for the presence of a component of the electric field of the radiation in the propagation direction. A set of equations for the evolution of the complex amplitudes of the radiation has been derived in the time domain, and converted to the frequency domain, where we consider many finite-width Fourier components of the radiation field, collectively extending across the full Zeeman pattern. A classical reduction of the frequency-domain equations leads to a set of nine coupled differential equations for the distance evolution of the standard Stokes parameters and five additional parameters that represent a coupling of the z-component of the electric field to the usual x and y components. These latter five parameters may represent radiation with orbital angular momentum (OAM).

There is a non-trivial coupling between the response of Zeeman-split molecules in a non-uniform magnetic field, and the electric field of radiation in the direction of propagation, and this

coupling is strongest when the magnetic field is perpendicular to the propagation direction. Although it is not obvious from the evolution equations, the standard reduction to a uniform field (setting the azimuthal angle $\phi' = 0$) results in radiation that may have polarization, but no OAM. This result was confirmed in Section 6.2. The OAM coupling is also most effective when, for a selected Fourier component or frequency, there is a large difference between the inversions in the various π- and σ-transitions of the Zeeman pattern. If we assume symmetric pumping, this implies that OAM generation will be significantly more efficient in molecules with a large Zeeman splitting (for example OH) than in closed-shell species (for example SiO, water and methanol).

A restricted analytical solution demonstrates that the coupling of the parameters representing OAM to the Stokes parameters, particularly Stokes-I, is non-trivial. For a suitable non-uniform magnetic field, in this case an ideal quadrupole, OAM can be generated from seed radiation without OAM or polarization, just as polarization may be so generated in a uniform field. Levels of OAM may grow large without the need for maser saturation.

A trial computational solution of the governing equations shows that in an intermediate amplification regime (intensity vastly greater than the background, but not saturating) OAM parameters may become large, at least with a non-uniform magnetic field of rather ideal structure. Maser radiation propagated perpendicular to the magnetic field may therefore evolve OAM fractions approaching 100 per cent. There is a hierarchy of amplification levels with Stokes-I and the OAM parameters J,G and H as the strongest set, followed by W, X and Stokes U, and finally a weakly amplified Stokes-V. Radiation patterns depart from usual OAM expectations owing to the exponential amplification of angular structure.

OAM conversion may partially account for the loss of linearly-polarized OH masers if non-uniform magnetic fields are common at the scales typical of resolved VLBI maser spots. Additional diagnostic value of OAM radiation, in the context of the present work, is discussed at the end of Section 6.2.

ACKNOWLEDGMENTS

Computations were carried out on the Legion supercomputer at the HiPerSPACE Computing Centre, University College London, which is funded by the UK Science and Technology Facilities Council (STFC).

REFERENCES

Akamatsu D., Kozuma M., 2003, Phys. Rev. A, 67, 023803
Allen L., Beijersbergen M. W., Spreeuw R. J. C., Woerdman J. P., 1992, Phys. Rev. A, 45, 8185
Allen L., Padgett M., 2011, The Orbital Angular Momentum of Light: An Introduction. Wiley-VCH Verlag GmbH & Co. KGaA, pp 1–12
Arfken G., 1970, Mathematical Methods for Physicists. Academic Press, 24/28 Oval Road, London, UK
Asensio Ramos A., Trujillo Bueno J., 2006, ApJ, 636, 548
Barnett S. M., 2002, Journal of Optics B: Quantum and Semiclassical Optics, 4, 7
Bazhenov V. Y., Soskin M. S., Vasnetsov M. V., 1992, Journal of Modern Optics, 39, 985
Beijersbergen M. W., Allen L., van der Veen H. E. L. O., Woerdman J. P., 1993, Optics Communications, 96, 123
Berestetskii V. B., Lifshitz E. M., Pitaevskii L. P., 1982, Quantum Electrodynamics, Second Edition: Volume 4. Course of theoretical physics, Butterworth-Heinemann
Deguchi S., Watson W. D., 1990, ApJ, 354, 649
Dinh-v-Trung 2009a, MNRAS, 396, 2319
Dinh-v-Trung 2009b, MNRAS, 399, 1495
Dousmanis G. C., Sanders T. M., Townes C. H., 1955, Physical Review, 100, 1735
Eisberg R., Resnick R., 1985, Quantum physics of atoms, molecules, solids, nuclei, and particles. Quantum Physics of Atoms, Molecules, Solids, Nuclei and Particles, Wiley
Elias II N. M., 2008, A&A, 492, 883
Elitzur M., 1996, ApJ, 457, 415
Elitzur M., 1998, ApJ, 504, 390
Enge H. A., Wehr M. R., Richards J. A., 1974, Introduction to atomic physics
Ewen H. I., Purcell E. M., 1951, Nature, 168, 356
Fish V. L., Reid M. J., 2006, ApJS, 164, 99
Flanders D. C., 1983, Applied Physics Letters, 42, 492
Fried D. L., 1998, Journal of the Optical Society of America A, 15, 2759
Garcia-Barreto J. A., Burke B. F., Reid M. J., Moran J. M., Haschick A. D., Schilizzi R. T., 1988, ApJ, 326, 954
Gatley I., Beattie D. H., Lee T. J., Jones T. J., Hyland A. R., 1984, MNRAS, 210, 565
Goldreich P., Keeley D. A., Kwan J. Y., 1973, ApJ, 179, 111
Goldreich P., Sridhar S., 1995, ApJ, 438, 763
Gray M. D., 2012, Maser Sources in Astrophysics. Cambridge University Press, Cambridge, UK
Gray M. D., Field D., 1994, A&A, 292, 693
Gray M. D., Field D., 1995, A&A, 298, 243
Green J. A., Gray M. D., Robishaw T., Caswell J. L., McClure-Griffiths N. M., 2014, MNRAS, 440, 2988
Grinter R., 2008, Journal of Physics B Atomic Molecular Physics, 41, 095001
Hamaker J. P., Bregman J. D., 1996, A&AS, 117, 161
Harwit M., 2003, ApJ, 597, 1266
Humblet J., 1943, Physica, 10, 585
Lavery M. P. J., Speirits F. C., Barnett S. M., Padgett M. J., 2013, Science, 341, 537
Littlefield T. A., Thorley N., 1979, Atomic and nuclear physics. an introduction
Maccalli S., Pisano G., Colafrancesco S., Maffei B., Richard Ng M. W., Gray M., 2013, Applied Optics, 52, 635
Marrucci L., Manzo C., Paparo D., 2006, Physical Review Letters, 96, 163905
Menegozzi L. N., Lamb Jr. W. E., 1978, Phys. Rev. A, 17, 701
Oesch D. W., Sanchez D. J., 2014, A&A, 567, A114
Oesch D. W., Sanchez D. J., Tewksbury-Christle C. M., 2012, Optics Express, 20, 1046
Padgett M., Courtial J., Allen L., 2004, Physics Today, 57, 050000
Press W. H., Teukolsky S. A., Vetterling W. T., Flannery B. P., 1992, Numerical recipes in FORTRAN. The art of scientific computing
Sanchez D. J., Oesch D. W., 2011a, Optics Express, 19, 25388
Sanchez D. J., Oesch D. W., 2011b, Optics Express, 19, 24596
Sanchez D. J., Oesch D. W., Reynolds O. R., 2013, A&A, 556, A130
Santamato E., 2004, Fortschritte der Physik, 52, 1141
Tamm C., Weiss C. O., 1990, Optics Communications, 78, 253
Watson W. D., Wyld H. W., 2001, ApJ, 558, L55
Weinreb S., Meeks M. L., Carter J. C., 1965, Nature, 208, 440

Western L. R., Watson W. D., 1984, ApJ, 285, 158
Wiebe D. S., Watson W. D., 2007, ApJ, 655, 275
Woodgate G. K., 1980, Elementary Atomic Structure